INVESTIGATING THE ROLE OF EUKARYOTIC INITIATION FACTOR 5B (EIF5B) IN ORAL SQUAMOUS CELL CARCINOMA

JINAY PATEL
Bachelor of Science, University of Lethbridge, 2021

A thesis submitted in partial fulfilment of the requirements for the degree of

MASTER OF SCIENCE
In
BIOCHEMISTRY

Department of Chemistry and Biochemistry
University of Lethbridge
LETHBRIDGE, ALBERTA, CANADA

INVESTIGATING THE ROLE OF EUKARYOTIC INITIATION FACTOR 5B (eIF5B) IN ORAL SQUAMOUS CELL CARCINOMA

JINAY PATEL

Date of Defense: July 8, 2024

Dr. Nehal Thakor Thesis Supervisor	Professor	Ph.D.
Dr. Pinaki Bose Thesis Examination Committee Member	Associate Professor	Ph.D.
Dr. Olga Kovalchuk Thesis Examination Committee Member	Professor	MD/Ph.D.
Dr. Bruce McKay External Examiner Carleton University Ottawa, Ontario	Professor	Ph.D.
Dr. Michael Gerken, Chair, Thesis Examination Committee	Professor	Ph.D.

ABSTRACT

Oral squamous cell carcinoma (OSCC) is a common malignancy of the mucosal epithelium affecting ~600,000 patients a year. Patient prognosis remains poor despite improvements in the therapeutic regime. Therefore, new therapeutic targets must be identified that improve the current standard of care. Regulation of mRNA translation plays a critical role in oncogenesis and cancer progression. Particularly, the IRES-mediated non-canonical translation of distinct mRNAs has been implicated in tumorigenesis. Eukaryotic initiation factor 5B (eIF5B) is a key factor that drives IRES-mediated translation of distinct anti-apoptotic proteins and is implicated in the pathophysiology of several malignancies. Single-cell RNAseq data analysis demonstrated that *EIF5B* is predominantly expressed in cancer cells compared to other cells in the tumor microenvironment. Further bioinformatic analyses revealed that higher *EIF5B* mRNA is correlated with poor patient prognosis for OSCC patients. Therefore, we aimed to establish the pre-clinical rationale for eIF5B as a therapeutic target for OSCC. Cell viability data suggested that RNAi-mediated eIF5B depletion significantly increased OSCC cell death under TRAIL treatment. eIF5B depletion also resulted in decreased levels of multiple antiapoptotic proteins. Bromodeoxyuridine (BrdU) incorporation, invasion, and wound healing assays suggested eIF5B depletion hinders proliferation, invasion and migration phenotypes, respectively. Western blot analysis revealed that proteins involved in ERK and NF-κB signalling, VEGF and HIF-1α, decreased upon eIF5B depletion. eIF5B depletion also resulted in the decrease of angiogenic biomarkers and endothelial tube formation, suggesting a role of eIF5B depletion in decreasing the angiogenic capability of OSCC cells. Stable eIF5B depletion was achieved with the use of shRNA. Under these conditions, eIF5B depletion increased cell death in the presence of cisplatin. Decreased invasion phenotypes were also observed using shRNA-mediated

knockdown, setting up the pipeline to transition experiments into preclinical mouse models. Thus, my work has a strong potential to establish eIF5B as a therapeutic target for OSCC treatment.

CONTRIBUTION OF AUTHORS

Contribution of Authors

Chapter 1. I wrote the introduction and Dr. Nehal Thakor provided edits and comments

Chapter 2. I wrote the methods and materials and Dr. Nehal Thakor provided edits and comments

Chapter 3. I wrote the results and Dr. Nehal Thakor provided edits and comments. Single-cell RNA sequencing data was generated and provided by Dr. Pinaki Bose (Figure 1). OSCC-specific patient survival curves were also generated and provided by Dr. Pinaki Bose (Figure 3B). Invasion assays in Cal33 cells using reverse-transfection and wound healing assays were performed by Pavan Lakshmi Narasimha. I received assistance from Dr. Nehal Thakor in writing the results and discussion.

Chapter 4. I wrote the discussion and Dr. Nehal Thakor provided edits and comments

ACKNOWLEDGEMENTS

I would like to start by thanking my thesis supervisor, Dr. Nehal Thakor for his support, guidance and mentorship through my 1 year of undergraduate study and 3 years of graduate studies in the Thakor lab where I have been encouraged and challenged to grow as a researcher.

I would also like to thank the members of my supervisory committee Dr. Pinaki Bose and Dr. Olga Kovalchuk for providing valuable feedback and suggestions. I would also like to thank Dr. Michael Gerken for chairing the defence and Dr. Bruce McKay for providing insight and guidance as an external examiner.

I would like to thank my lab mates Pavan, Veda, Tithi, and Hannah who have provided valuable assistance, guidance and support. I would also like to thank Dr. Roy Golsteyn and his lab for assistance with phase contrast microscopy.

I would also like to thank my family, loved ones, and community who have been incredibly loving towards me and provided great support.

TABLE OF CONTENTS

LIST OF TABLES

LIST OF FIGURES

Chapter 1

Chapter 3

LIST OF ABBREVIATIONS

5’m7G cap- 5’ methylated guanine cap
ASAP1- ArfGAP with SH3 domain, ankyrin repeat and PH domain 1
Bcl-xL- B-cell lymphoma-extra large
BrdU- Bromodeoxyuridine
CD95- Cluster of differentiation 95
cFLIP- cellular FLICE-inhibitory protein
$cFLIP_L$- large isoform of cFLIP
$cFLIP_s$- short isoform of cFLIP
cIAP1- cellular inhibitor of apoptosis protein 1
Cyt C- Cytochrome c
DAB- 3,3-diaminobenzidine
DAPI- 4’,6-diamidino-2-phenylindole
DISC- death-inducing signaling complex
DMEM- Dulbecco’s high-modified Eagle’s medium
DMSO- Dimethylsulfoxide
DNA- Deoxyribonucleic acid
DPX- Dibutylphthalate polystyrene xylene
DR4- Death receptor 4
DR5- Death receptor 5
EGFR- Epidermal growth factor receptor
eIF1- Eukaryotic initiation factor 1
eIF1A- Eukaryotic initiation factor 1A
eIF2- Eukaryotic initiation factor 2
eIF2A- Eukaryotic initiation factor 2A
eIF2B- Eukaryotic initiation factor 2B
eIF2D- Eukaryotic initiation factor 2D
eIF2α- Eukaryotic initiation factor 2 alpha
eIF3- Eukaryotic initiation factor 3
eIF4A- Eukaryotic initiation factor 4A
eIF4E- Eukaryotic initiation factor 4E
eIF4G- Eukaryotic initiation factor 4G
eIF5B- Eukaryotic initiation factor 5B
eIFs- Eukaryotic initiation factors
EL-1- Endothelin 1
ERK 1/2- Extracellular signal-regulated kinase ½
ERK- Extracellular signal-regulated kinase
FADD- FAS-associated death domain protein
Fas-L- Fas ligand
GBM- Glioblastoma multiforme
GEPIA 2- Gene expression profiling interactive analysis 2
GFP- Green fluorescent protein
GTP- Guanosine triphosphate
HIF-1α- Hypoxia-inducible factor-1 alpha

HNSCC- head and neck squamous cell carcinoma
HPV- Human papillomavirus
HRP- horseradish peroxidase
HUVEC- Human umbilical vein endothelial cells
IAPs- Inhibitor of apoptosis proteins
IF2- Initiation factor 2
IKKB- Inhibitor of nuclear factor kappa B kinase subunit beta
IL-8- Interleukin 8
IRES- Internal ribosome entry site
IκB- inhibitor of NF-κB
MAPK- Mitogen-activated protein kinase
M-CSF- Macrophage colony-stimulating factor
Met-tRNAi- methylated initiator transfer RNA
mRNA- Messenger ribonucleic acid
NF-κB- Nuclear factor kappa B
OSCC- Oral squamous cell carcinoma
p-EGFR- Phosphorylated EGFR
p-ERK ½- Phosphorylated ERK ½
p-NF-κB- Phosphorylated NF-κB
PBS- Phosphate-buffered saline
PD-L1- Programmed cell death ligand 1
PLGF- Placental growth factor
RASK 1-4- Ribosomal S6 kinases 1-4
RiboSeq- Ribosome profiling
RIPA- radioimmunoprecipitation assay
RNA seq- Single-cell RNA sequencing
ROS- Reactive oxygen species
RPG- Revolutions per minute
SDS-PAGE- Sodium dodecyl sulfate polyacrylamide gel electrophoresis
SEM- Standard error of the mean
shRNA- Short hairpin RNA
siRNA- Small interfering RNA
SMACs- second mitochondrial-derived activators of caspases
tBid- Truncated Bid
TBS- Tris-buffered saline
TCGA- The cancer genome atlas
TMA- Tissue microarray
TNF- Tumor necrosis factor
TNFR1- tumor necrosis factor 1
TRAIL- TNF-related apoptosis-inducing ligand
UTR- Untranslated region
VEGF- Vascular endothelial growth factor
XIAP- X-lined inhibitor of apoptosis
EMT- Epithelial-mesenchymal transition
NIK- NF-κB-inducing kinase

CHAPTER 1

Investigating the role of eukaryotic initiation factor 5B (eIF5B) in oral squamous cell carcinoma

Introduction

Introduction

1.1 Overview of OSCC

Oral squamous cell carcinoma (OSCC) is the most common cancer of head and neck malignancies, accounting for up to 90% of cancers in the oral cavity (Pires et al, 2013, Yang et al, 2023, Cui et al, 2023, Rahadiani et al, 2023). OSCC affects approximately 600,000 patients per year [1], with about 30,000 people diagnosed in North America each year [2] [3,4]. OSCC occurrences are found in the tongue, tonsils, floor of the mouth, and soft palate (Figure 1.1) (Anwar et al, 2020, Pires et al, 2013). Key risk factors associated with OSCC include tobacco use, alcohol consumption, exposure to carcinogens, heritable predisposition, diet and human papillomavirus (HPV) infection (Nokovitch et al, 2023, Palve et al, 2018, Wu et al, 2022) [3]. OSCC tumors are heterogeneous with six different variants recognized being classified according to aspects such as invasive margins, the ratio of keratinized cells, nuclear polymorphisms, the grade of cancer, and the intensity of inflammation [4]. Continual exposure to these risk factors leads to genetic and epigenetic alterations, dysregulated tumor environment (eg, hypoxia) and improper activation of oncogenic pathways [3]

1.2 Clinical challenge in OSCC treatment

OSCC is recognized as an aggressive cancer with a high mortality rate [3,5], ranging from 10% in early stages to 70% in later stages [6]. Treatment for OSCC includes a combination of therapy (Elsaady et al, 2023) of radiation (Lang et al, 2023) and surgical resection (Bajwa et al, 2020). The prognosis for OSCC patients is unfavorable (Ferreira et al, 2021) and is dependent upon the anatomical location and metastasis status of cancer (Al-Rawi et al, 2023), and if it is HPV positive or negative, with HPV-positive cancers being associated with a better prognosis [7]. Despite advances in treatment, the prognosis for OSCC remains unfavorable (Ferreira et al,

2021), with the 5-year survival rate estimated to be about 50% (Davaatsend et al, 2023). Given the poor outlook for patients, it is imperative that additional therapeutic targets be investigated. A key hallmark of many malignancies is the ability to resist and avoid apoptotic cell death with the aid of several different antiapoptotic proteins [8,9]. Therefore, the ability to reduce and regulate the level of these antiapoptotic proteins serves as a valuable opportunity to identify such therapeutic targets.

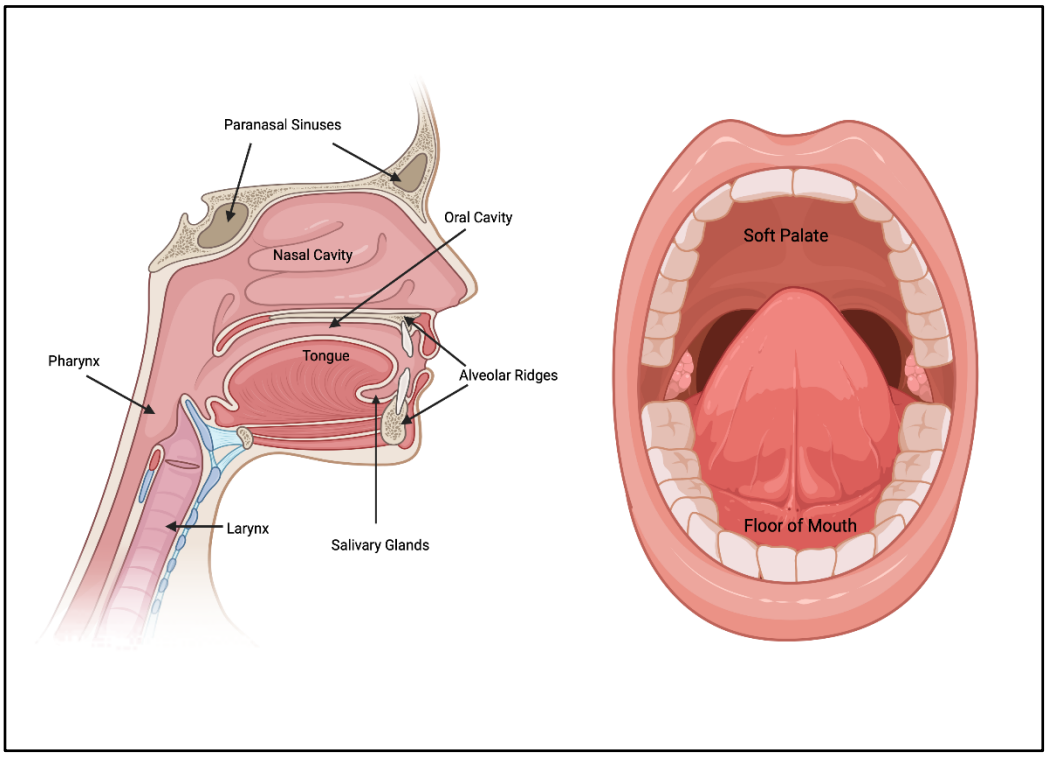

Figure 1.1. Visual schematic showing anatomical locations of OSCC. Image generated with BioRender

1.3 An overview of apoptosis

Apoptosis is an intricate, preprogrammed cell death program whose function is to ensure homeostasis in multicellular organisms by eliminating damaged, obsolete, or potentially

dangerous cells [10-12]. Apoptosis is activated by interaction with receptors on the cell surface, referred to as extrinsic apoptosis, or when pro-apoptotic proteins cause the permeabilization of the outer mitochondrial membrane, referred to as the intrinsic apoptotic pathway [12].

1.3.1 Extrinsic apoptosis

Extrinsic apoptosis is initiated by the binding of a death receptor ligand to death receptors of the tumor necrosis factor (TNF) gene family such as tumor necrosis factor receptor 1 (TNFR1), cluster of differentiation 95 (CD95), and TNF-related apoptosis-inducing ligand (TRAIL)-R1 and TRAIL-R2 [13-16]. Upon ligand binding (eg, tumor necrosis factor (TNF), Fas-L (Fas ligand), TRAIL), a multiprotein complex called death-inducing signaling complex (DISC) is formed, consisting of a Fas-associated death domain, procaspase-8, procaspase-10, and the antiapoptotic protein cellular FLICE-inhibitory protein (cFLIPs) [17-19]. DISC dimerization causes the self-proteolysis of procaspase-8, releasing the activated caspase 8 into the cytosol [19,20], where it can cleave procaspase-3 and -7 into their active caspase form, leading to the induction of apoptosis [21]. Another role of cytosolic caspase-8 is to cleave a BH3-only protein called Bid, allowing the truncated Bid (tBid) to translocate to the mitochondria [22], leading to activation of the Bcl-2 effectors BAX and BAK at the mitochondrial outer membrane [23,24]. This leads to permeabilization of the mitochondrial membrane, allowing cytochrome c (Cyt C) and second mitochondrial-derived activators of caspases (SMACs) to enter the cytosol [19,25,26]. SMACs inhibit inhibitor of apoptosis proteins (IAPs), allowing cytochrome c to form the apoptosome, which is a quaternary platform that activates procaspase-9 which then activates caspases -3,-6, and -7, leading to apoptotic cell death (Figure 1.2) [19,27].

1.3.2 Intrinsic apoptosis

Intrinsic apoptosis is triggered by various cellular stressors, such as DNA damage, hypoxia or cytotoxic drug treatment [19,28,29]. These stressors stimulate an increase in p53 production, resulting in increased Bax/Bak localization to the mitochondrial outer membrane and its subsequent polarization, leading to SMAC and cytochrome c release [19,28] and allowing the apoptosis pathway to proceed as described above (Figure 1.2).

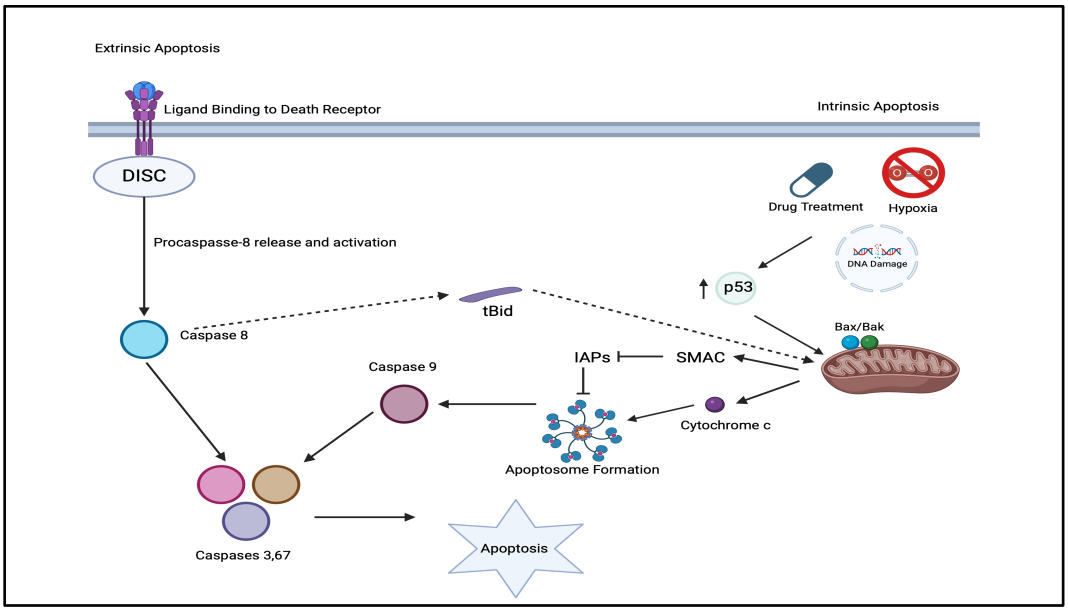

Figure 1.2. Visual schematic displaying the sequence of events in extrinsic and intrinsic apoptosis. Image generated with BioRender

1.4 Role of antiapoptotic proteins in apoptosis

Apoptosis is a highly regulated process to ensure that is activated at appropriate times and is executed carefully and efficiently [30]. One method of regulating apoptosis is with antiapoptotic proteins that aid in preventing extrinsic and intrinsic apoptosis. As mentioned above, cFLIP is an antiapoptotic protein found in two isoforms, a long isoform ($cFLIP_L$) and a short isoform ($cFLIP_s$), that is a component of the DISC and regulates extrinsic apoptosis [31]. cFLIP is found overexpressed in many malignancies and functions by sterically inhibiting FAS associated death

domain protein (FADD), the activator of caspase-8 [32,33]. cFLIP has also been suggested to interact directly with caspase-8, caspase-10 and death receptor 5 (DR5) to aid in evasion of apoptosis [17]. The cellular inhibitor of apoptosis protein 1 (cIAP1) is another antiapoptotic protein that aids in apoptotic resistance by competitively inhibiting the activation of caspases [34]. X-linked inhibitor of apoptosis (XIAP) is a multi-domain antiapoptotic protein that interacts with caspases 3,7, and 9 to inhibit the apoptotic cascade [35,36]. Another antiapoptotic protein of note is B-cell lymphoma-extra large (Bcl-xL), a member of the Bcl-2 family located in the membrane [37]. Bcl-xL sequesters pro-apoptotic members of the Bcl-2 family such as Bax and Bak [38]; this inhibits cytochrome c and SMAC release from the mitochondria, thus preventing apoptosome formation and XIAP inactivation.

1.5 Overview of invasion, migration, proliferation, and angiogenesis

In addition to evading apoptosis, additional hallmarks of cancer formation and progression include evasion of growth suppression mechanism, establishing replicative immortality, sustained proliferative signalling, angiogenesis, and invasion and migration [39-41]. Proliferation is a fundamental requirement for organismal growth and homeostasis which is tightly regulated through the progression of the cell cycle [42,43]. Normal tissues tightly regulate production and release of pro-growth factors that guide cells through growth and division [41]. Dysregulation of this process results in uncontrolled growth and cell division, a key step in tumor formation, particularly with the aid of increased production of growth factors that bind cell membrane receptors [41,44]. Angiogenesis is the process by which vascular tissue is formed to provide cells with valuable nutrients and oxygen as well as remove wastes [41]. Migration and invasion are the processes by which cells dissolve the surrounding extracellular matrix and spread into the surrounding tissue and/or distant sites, a process referred to as metastasis [45,46]. A well

characterized event in the process of invasion and metastasis is a decrease in E-cadherin a molecule that aids in cell-cell adhesion [41].

1.5.1 Overview of ERK signaling pathway

A central signalling pathway whose aberrant regulation is known to drive invasion, migration, and proliferation is the extracellular signal-regulated kinase/mitogen-activated protein kinase (ERK/MAPK) pathway [47,48]. This is a signalling pathway that is sequentially activated via phosphorylation [48]. The binding of mitogens or growth factors to their cell membrane receptors (eg, epidermal growth factor receptor (EGFR), the canonical activator Ras-ERK signalling) results in their activation via phosphorylation forming phosphorylated EGFR (p-EGFR), leading to downstream activation of Ras and Raf, which in turn phosphorylate and activate ERK1/2, forming phosphorylated ERK (p-ERK1/2) [48-51]. p-ERK 1/2 in turn aids in the activation of transcription factors such as ribosomal S6 kinases (RSK 1-4) [52] [48,53]. Another driver of proliferation to mention is hypoxia-inducible factor-1 alpha (HIF-1α), as it is stabilized in hypoxic environments and has been reported to support the adaptation of tumor cells to hypoxic environments, which has been reported in early tumor development [43,54]. HIF-1α has also been detected in normoxic conditions in neuroblastoma cells where it was suggested to play a role in metabolic regulation to promote the viability of tumor cells [55].

1.5.2 Overview of NF-kB signaling pathway

Nuclear factor kappa B (NF-κB) is a protein transcription factor that modulates cellular activities whose aberrant activity has been linked to cancer [56]. The NF-κB transcription factor family is composed of five proteins: p65, also called RelA, RelB, c-Rel, p105/50 (NF-κB1), and p100/52 (NF-κB2) [57]. The NF-κB signalling pathway can occur via a canonical pathway or non-canonical pathway [58]. In the canonical pathway, p65/p50 heterodimers are crucial for the

transcriptional regulation of target genes [58]. Under steady-state conditions, NF-κB is typically sequestered in the cytoplasm and is inhibited by an inhibitor of NF-κB (IκB) proteins [58,59]. The canonical pathway can be activated by the binding of a diverse array of immune receptors [60]. Ligand binding leads to the eventual degradation of IκB, resulting in NF-κB dimer activation via phosphorylation (p-NF-κB) and translocation to the nucleus [58].

In non-canonical NF-κB signalling, the binding of ligands from a subset of the tumor necrosis factor receptor (TNFR) family leads to a signalling cascade in which activation of NF-κB-inducing kinase (NIK) leads to the processing of p100 to p52; the p52/RelB dimers then translocate to the nucleus where they promote transcription of target genes [60,61].

Constitutive NF-κB activity has been reported in multiple human cancers where it has been suggested to promote tumor cell proliferation, suppress apoptosis and facilitate invasion [62]. NF-κB is also associated with angiogenesis, another hallmark of cancer in which the formation of new blood vessels plays a crucial role in tumor growth and invasion [62,63]. In addition to NF-κB, vascular endothelial growth factor (VEGF) is the most typical regulator of angiogenesis in tumors [63]. There has been reported cross-talk between ERK and NF-κB signalling pathways. ERK activation has been associated with phosphorylation of p65, leading to its subsequent phosphorylation (p-NF-κB) and activation [64]. VEGF, in addition to being a key promoter of angiogenesis, has been reported to activate ERK signaling [65]

1.6 Addressing the clinical challenge with mRNA translation machinery

Aberrant mRNA translation has been strongly linked with oncogenesis and tumor progression [66-68]. Directly relevant to my research project, the expression of distinct anti-apoptotic proteins is regulated at the mRNA translation level [17,69,70], which in turn allows cancer cells to resist cancer

therapeutics [8]. As the current standard of care for OSCC has limited success in the clinic[71], the mRNA translation machinery may provide an opportunity to identify novel therapeutic targets for the treatment of OSCC

1.7 Overview of translation and translation initiation

Translation initiation, the process by which messenger RNA (mRNA) is translated from the nucleic acid code to the protein amino acid code, is a highly regulated and complex process, requiring the action of at least 12 different initiation factors [72]. These initiation factors play key roles in the translation of mRNAs and are crucial components of several cell signalling pathways (Hinnebush et al, 2012, Hao et al, 2020). Under normal growth conditions eukaryotic cells mostly utilize a canonical translation initiation process (see below) (Sharma et al, 2016). However, under pathophysiological stress conditions, the canonical translation initiation is attenuated due to modifications of critical eukaryotic initiation factors (eIFs) [73,74]. Importantly, certain mRNAs circumvent the global mRNA translation attenuation and continue to be translated via non-canonical translation mechanisms [73,75]. These mRNAs can encode distinct cell survival proteins such as anti-apoptotic proteins. Thereby, the non-canonical translation process can provide critical cell survival advantages to the cell under pathophysiological stress conditions such as cancer.

1.8 Canonical translation initiation

Canonical translation initiation, or cap-dependent translation is a complex process requiring more than 25 different proteins, including at least 12 initiation factors (Sharma et al, 2016, Hinnebusch et al, 2012). Canonical translation initiation begins with the formation of the

eIF4F complex consisting of three different initiation factors: the cap-binding factor eIF4E, the scaffold protein eIF4G, and the eIF4A helicase onto the 5'm7G cap on mRNA (Sharma et al, 2016). The ternary complex, consisting of eIF2, GTP and the met-tRNA*i,* interacting with the 40S ribosomal subunit, is then brought to the 5' mRNA end via connection with eIF4G. This connection is facilitated by eIF3 and assisted by eIF1A and eIF1 [75], resulting in the formation of the 43S preinitiation complex (Sharma et al, 2016). The ternary complex then scans along the mRNA in search of an AUG start codon in the optimal context for translation to begin. This is obtained with the help of the eIF4A helicase, eIF1, eIF1A and eIF3 (Sharma et al, 2016). eIF1 binds to the P site of the 40S subunit and prevents met-tRNA*i* incorporation into the P site during the scanning phase (Sharma et al, 2016, Yi et al, 2022). In addition to working together with eIF1A to facilitate the binding of the preinitiation complex onto the start codon, eIF1 also prevents premature GTP hydrolysis by eIF2α (Sharma et al, Yi et al, 2022). Upon binding to the optimal start codon, two additional initiation factors, eIF5 and eIF5B, mediate the hydrolysis of GTP by the GTPase eIF2α, causing the release of bound initiation factors (Sharma et al, 2016). This results in the start codon being placed in the P site with the initiator tRNA and allows the 60S ribosomal subunit to bind with the aid of eIF5B, creating a functional 80S initiation complex that can proceed onto elongation (Sharma et al, 2016). To facilitate further initiation, an initiation factor named eIF2B recharges the spent GDP on eIF2α with GTP (Figure 1.3) (Sharma et al, 2016).

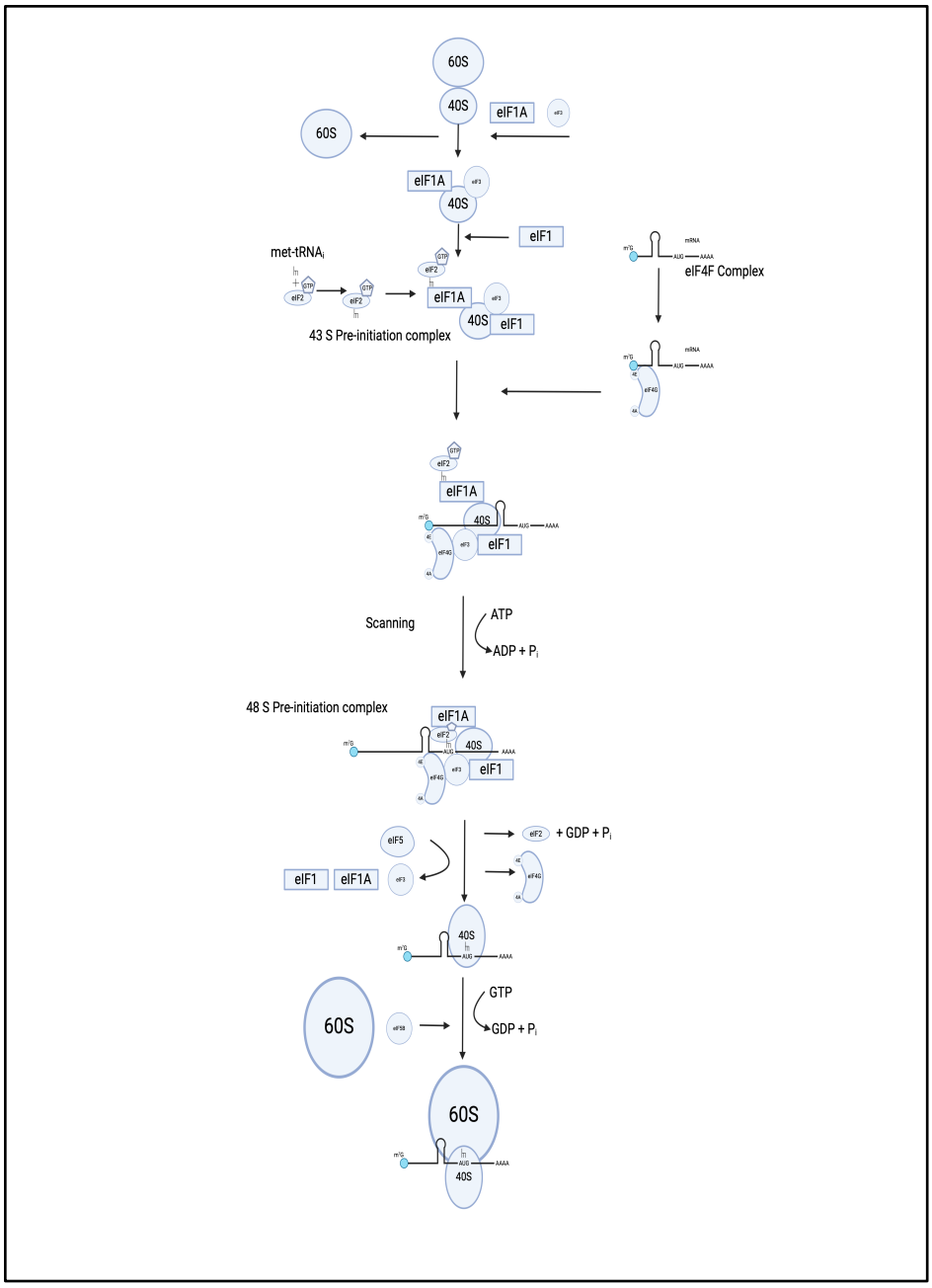

Figure 1.3. Visual Schematic displaying the process of canonical translation initiation. Image generated with BioRender

1.9 Shift from canonical translation initiation to non-canonical translation initiation and IRES elements

Under conditions of stress, such as nutrient deprivation or hypoxia, the process of translation initiation undergoes a shift from canonical to non-canonical, or cap-independent translation initiation (Sharma et al, 2016). One of the key events causing the shift to non-canonical translation initiation is the kinase-mediated phosphorylation of the initiation factor eIF2α, preventing the ability of eIF2α to deliver met-tRNAi to the 40S ribosome [76]. This phosphorylation event leads to the halting of global protein synthesis and the activation of alternative translation mechanisms. One such mechanism involves the use of internal ribosome entry site (IRES) elements (Sharma et al, 2016, Martinez-Salas et al, 2017).

IRES elements were originally discovered in the genomic RNA of viruses that lack 5' cap structures, such as poliovirus and encephalomyocarditis viruses, but have also been found in eukaryotic RNAs; for example, an estimated 10% of mammalian mRNAs have elements that function as IRESs [31,77-80]. IRES elements are cis-acting regulatory regions of RNA that can recruit the 40S ribosomal subunit without relying on the 5' cap structure [77,78,81,82]. Interestingly, IRES elements are found in the 5' untranslated region (UTR) of mRNAs encoding distinct anti-apoptotic proteins such as XIAP, Bcl-xL, cIAP1, and $cFLIP_s$. Additionally, the translation of mRNAs encoding the critical angiogenesis and invasion regulators such as vascular endothelial growth factor (VEGF) and hypoxia-inducible factor 1-alpha (HIF-1α) have also been known to be translated from IRES elements [83,84]. Therefore, the regulation of mRNA translation via an IRES-mediated mechanism has a strong potential to govern cellular processes involved in tumorigenesis.

1.10 Noncanonical Translation Initiation

As previously mentioned, eIF2α phosphorylation caused by cellular stress attenuates general protein synthesis and inhibition of cap-dependent translation by inhibiting delivery of met-tRNAi to the 40S ribosome [77]. However, translation initiation on a pool of mRNAs switches from canonical to non-canonical mode, which allows translation of a subset of IRES-containing mRNAs under stress conditions. A body of work has identified eIF5B as a key driver of IRES-mediated translation initiation as its depletion was associated with the decrease in proteins whose mRNAs harbor IRES elements such as XIAP, Bcl-xL, and cIAP1 [31,75,76]. Normally, eIF5B facilitates the association of 40S and 60S ribosomal subunits during canonical translation [73]. However, eIF5B, a homologue of bacterial initiation factor 2 (IF2) [85], appears to have other functions. Notably, eIF5B can deliver and stabilize initiator-tRNA independent of eIF2 [85]. Thus, eIF5B parallels the role of eIF2 under stress conditions. As such, eIF5B forms an alternative ternary complex (eIF5B-GTP-Met-tRNAi) and delivers initiator tRNA during the IRES-mediated translation initiation (Figure 1.4) [75]

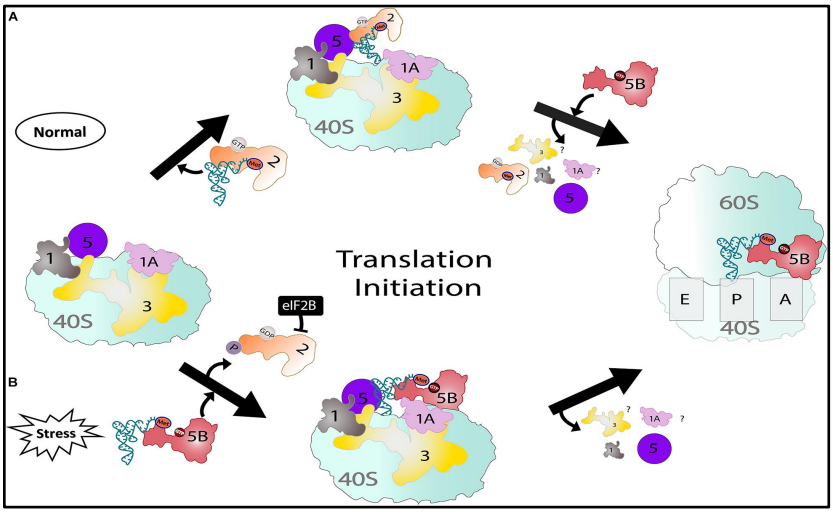

Figure 1.4. Two pathways of met-tRNAi delivery to P-site of 40S ribosome. Under canonical translation initiation (A), eIF2 delivers the initiator tRNA. However, when eIF2α is phosphorylated, eIF5B takes the role of eIF2 in delivering tRNA. Image obtained from Chukka et al, 2021 (CC-BY Creative Commons Attribution License)

1.11 Role of eIF5B in cancer

The influence of eIF5B in the survival, proliferative, migratory, and invasive capabilities of multiple cancers has been investigated. In glioblastoma cells, eIF5B expression was associated with resistance to apoptosis, and eIF5B depletion increased the susceptibility of glioblastoma cells to TRAIL-mediated apoptotic death by reducing levels of the antiapoptotic proteins mentioned above (Figure 1.5) [31]. Interestingly, depleting eIF5B in a non-cancerous cell line had no significant impact on viability or susceptibility to apoptosis [31]. In prostate cancer, eIF5B expression was correlated with poor immune response sensitivity via high expression of PD-L1 [86] [87]. eIF5B depletion resulted in decreased proliferative capabilities in prostate cancer cells and increased sensitivity to apoptosis [86]. A similar relationship between eIF5B and PD-L1 was established in lung cancer [88]. In hepatocellular carcinoma cells, eIF5B was shown to promote proliferation and invasion by increasing levels of ASAP1; these effects were reversed upon eIF5B depletion [89].

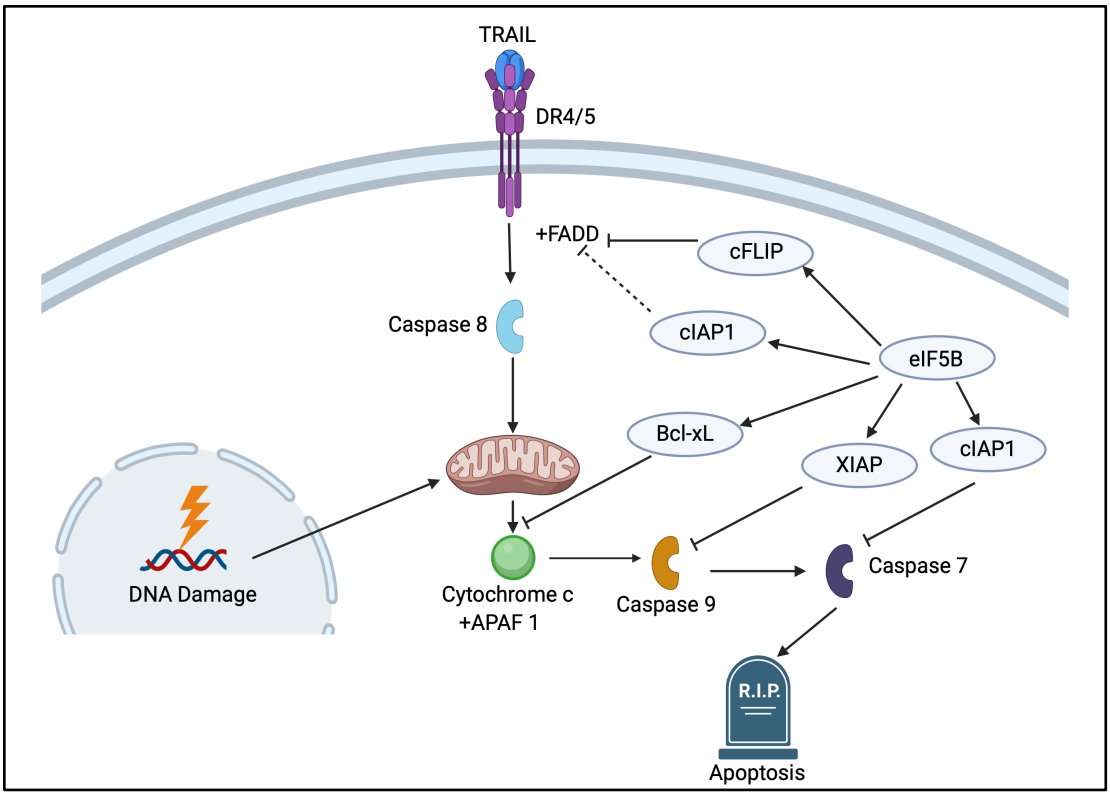

Figure 1.5. eIF5B regulates IRES-mediated translation of the antiapoptotic proteins cIAP1, XIAP, Bcl-xL and cFLIP. The expression of these proteins in turn promotes resistance to intrinsic and extrinsic apoptotic cell death. The depletion of eIF5B is correlated with decreased levels of these proteins and increased sensitivity to TRAIL [31]. As shown in the results section of my thesis, eIF5B transcript and eIF5B protein are expressed at a higher level in OSCC cells compared to other cells in OSCC tumors. Additionally, eIF5B is associated with poor prognosis in OSCC patients. Therefore, the overarching goal of my thesis is to establish the pre-clinical rationale for targeting eIF5B for OSCC treatment. Image generated with BioRender

1.12 Project objective and hypothesis

Given the role of eIF5B in the IRES-mediated translation of proteins involved in cell survival under stress conditions, and the established influence of eIF5B in the survival of multiple malignancies, the overarching objective of my project is to establish the pre-clinical rationale for eIF5B as a therapeutic target in OSCC. *I hypothesize that eIF5B depletion will increase apoptotic cell death in OSCC Cal33 by decreasing the IRES-mediated translation of antiapoptotic proteins. I also hypothesize that eIF5B depletion will result in a decrease in*

proteins involved in proliferative, invasive and migratory pathways, leading to inhibited invasion, proliferation, and migration upon eIF5B depletion. Accordingly, I have focused my study on the following three aims.

Aim 1: To define the role of eIF5B in OSCC cell survival.

Aim 2: To define the role of eIF5B in proliferation, angiogenesis, and invasion and migration of OSCC cells.

Aim 3: To establish the pipeline (validate reagents) for studying the role of eIF5B in OSCC using an orthotopic xenograft mouse model.

CHAPTER 2- Material and Methods

Methods and Materials

2.1 Cell Culture and Reagents

Cal33 (OSCC tongue carcinoma, provided by Dr. Pinaki Bose) and BJ5TA (immortalized fibroblast, provided by Dr. Igor Kovalchuk) cell lines were propagated in Dulbecco's high-modified Eagle's medium (DMEM, HyClone) with 4mM L-glutamine, 4,500 mg/L glucose, and 1 mM sodium pyruvate, supplemented with 10% heat-inactivated fetal bovine serum (Gibco) and 1% penicillin-streptomycin (Gibco). Cells were incubated at 37°C in an incubator supplemented with 5% CO_2. Reverse transfections were performed using Lipofectamine RNAiMAX (Invitrogen) according to the manufacturer's instructions and scrambled non-specific negative control siRNA (siC; Quiagen) and Stealth RNAi^{TM} siRNA targeting eIF5B (HSS114469/70/71; Invitrogen. Transductions were performed using a scrambled control shRNA (shC, provided by Dr. Donna Senger lab) or an shRNA specific for eIF5B (sh30, sequence:5'AAACCCAGGGCTGCCTTGGAAAAG - 3', from Horizon, https://horizondiscovery.com/en/gene-modulation/knockdown/shrna/products/trc-lentiviral-shrna?nodeid=entrezgene-9669). Cal33 cells were seeded in media containing 3µg/mL polybrene and 250µL lentivirus. 24 hours after transduction, 2µg/mL puromycin was added. Cells were incubated for 48-72 hours to allow for successful selection.

2.2 Cell Viability Assay

Cal33 and BJ5TA were seeded at 1,000 cells/well. After 24-48 hours of incubation, cells were treated with 100 ng/mL TRAIL. After 72 hours, alamarBlue was added and absorbances (excitation at 560nm; emission at 590nm) were measured after 17 more hours using a Cytation 5 plate imager (BioTek). TRAIL was obtained from Millipore-Sigma.

Moreover, Cal33 cells were transduced with either a scrambled control shRNA (shC) or shRNA specific for eIF5B (sh30) and 150,000 cells/well were seeded in a 6-well plate in media supplemented with 2 μg/mL puromycin. Upon successful puromycin selection, 3,000 cells/well were seeded in a 96-well plate. 24 hours after incubation, 20 μM cisplatin or 2μL dimethyl sulfoxide (DMSO; vehicle control for cisplatin, corresponding to 20 μM cisplatin) was added. After 72 hours, alamarBlue was added and the absorbance was measured after 17 more hours using a Cytation 5 plate imager.

Cisplatin Kill Curve

Cal33 cells were transduced and seeded into a 96-well plate as described above. 24 hours after seeding, cisplatin was added at concentrations ranging from 0 to 30 μM in 2 μM increments while 2μL DMSO was added to the 0μM wells as a vehicle control. After 72 hours, alamarBlue was added and absorbances were measured after 17 more hours using a Cytation 5 plate imager.

2.3 Western Blotting

Cal33 and BJ5TA cells were seeded at 100,000 cells/well in a 6-well plate and reverse transfected. 100ng/mL TRAIL was added 92 hours after transfection and harvested after 4 more hours. Cells were harvested in radioimmunoprecipitation assay (RIPA) lysis buffer with protease inhibitors. Equal amounts of proteins (typically 20 μg; 40 μg for $cFLIP_s$ and cleaved caspase 7) were resolved by sodium dodecyl sulfate polyacrylamide gel electrophoresis and transferred onto 0.2 μm nitrocellulose membrane (GE Healthcare). Individual proteins were detected by immunoblotting with the antibodies listed in Table 1. Nitrocellulose membranes were blocked with milk powder (typically 10% wt/vol; 1% wt/vol for $cFLIP_s$ and cleaved caspase 7) dissolved

in 0.1% phosphate buffer saline. Immunoblots were imaged in an AI600 image (GE Healthcare) and densitometry was performed using the AI600 analysis software.

Antibodies Used in Western Blotting

Table 1. Vendor Information for Antibodies Used in Western Blotting

Company	Antibody Target	Catalogue Number
Abcam	Secondary: Goat anti-rabbit-HRP conjugate	ab97051
ProteinTech	eIF5B	13527-1-AP
Bio-Rad	β-actin (hFAB Rhodamine)	12004163
Cell Signalling Technologies	Bcl-xL	2764
	cIAP1	7065
	Caspase 7	12827
	DR4	42533
	DR5	69400
	FLIP	56343
	EGFR	4267
	p-EGFR	3777
	ERK	9102
	p-ERK	4695
	HIF-1α	3716
	NFκB	4764
	p-NF-κB	3031
	XIAP	14434
Invitrogen	VEGFA	JH121

2.4 BrdU Incorporation Assays

Cal33 and BJ5TA cells were seeded at 1,000 cells/well and reverse-transfected in a 96-well plate. After 48 hours of incubation, 1x BrdU was added according to the manufacturer's instructions. After a further 48 hours cells were fixed with fixing solution provided by the manufacturer and absorbance readings were taken at 450 nm and 550nm using a Cytation 5 plate imager according to the manufacturer's instructions.

2.5 Invasion Assays

24 hours before beginning the assay, spent media was removed from Cal33 cells and replaced with serum-free media. Cal33 cells were then seeded at 100,000 cells/well and reverse-transfected with either a scrambled control siRNA (siC) or siRNA specific for eIF5B (si5B) into collagen inserts in a 24-well plate in serum-free media with serum-containing media on the other side of the insert. Cells were incubated for 48 hours before cell staining and extraction were performed according to the manufacturer's instructions (QCM Collagen Cell Invasion Assay, 24-well 8µm, calorimetric; ECM551 from Sigma Aldrich).

Additionally, Cal33 cells were transduced with either a scrambled control shRNA (shC) or shRNA specific for eIF5B (sh30) and 150,000 cells/well were seeded in a 6-well plate in media supplemented with 2 µg/mL puromycin. Upon successful puromycin selection, media was removed, and cells were washed with 1x phosphate-buffered saline (PBS) wash buffer and supplemented with serum-free media 24 hours before beginning the assay. Cells were then split in serum-free media into the collagen inserts with serum-containing media on the other side of the insert. Cells were incubated for 48 hours before cell staining and extraction were performed according to the manufacturer's instructions (QCM Collagen Cell Invasion Assay, 24-well 8µm, calorimetric; ECM551 from Sigma Aldrich).

2.6 Wound Healing Assays

Cal33 cells were reverse-transfected with either a scrambled control siRNA (siC) or siRNA specific for eIF5B (si5B). After reaching appropriate confluency, a scratch was introduced using a P10 pipette tip. Brightfield and phase-contrast images were taken using the Cytation 5 plate reader at the time of scratch introduction and 24 hours after. Wound healing was analyzed using ImageJ wound healing macro.

2.7 Angiogenic Biomarker Analysis

Cal33 and BJ5TA were seeded at 100,000 cells/well and reverse-transfected in a 6-well plate. After 72 hours of incubation, the media was removed, washed with 1x PBS, and replaced with serum-free media 24 hours before harvesting. 4 hours before harvesting, 100 ng/mL TRAIL was added. Spent media was collected and centrifuged at 3,000 revolutions per minute (rpm) (Thermo Scientific ST 8R) for 2 minutes. Media was stored and frozen at -80°C and shipped to Eve Technologies for the Human Angiogenesis & Growth Factor 17-Plex Discovery Assay® Array (HDAGP17). The multiplexing analysis was performed using the Luminex™ 200 system (Luminex, Austin, TX, USA) by Eve Technologies Corp. (Calgary, Alberta). Seventeen markers were simultaneously measured in the samples using Eve Technologies' Human Angiogenesis & Growth Factor 17-Plex Discovery Assay® (MilliporeSigma, Burlington, Massachusetts, USA) according to the manufacturer's protocol. The 17-plex consisted of Angiopoietin-2, BMP-9, EGF, Endoglin, Endothelin-1, FGF-1, FGF-2, Follistatin, G-CSF, HB-EGF, HGF, IL-8, Leptin, PLGF, VEGF-A, VEGF-C, VEGF-D. Assay sensitivities of these markers range from 0.2 – 42.8 pg/mL for the 17-plex. Individual analyte sensitivity values are available in the MilliporeSigma MILLIPLEX® MAP protocol.

2.8 Endothelial Tube Formation Assays

Human umbilical vein endothelial cells (HUVEC) were seeded at 50,000 cells/well in a 96-well plate coated with Matrigel. Cells were supplemented with spent Cal33 media collected for the angiogenic biomarker assay. Branch formation was allowed to take place for 8 hours. Brightfield microscopy images were taken at 4-hour and 8-hour intervals. One well per condition

was imaged and collected by taking images with a Cytation 5 plate imager. Analysis of tube formation characteristics was performed using ImageJ using available angiogenesis macro.

2.9 Tissue Microarray Analyses

Slides were deparaffinized in xylene followed by ethanol washes of differing concentrations (100%-70%) followed by a final wash in H_2O. Antigen retrieval was performed by placing slides in antigen retrieval buffer (10mM Citrate buffer pH 6.0 + 0.05% Tween 20) and microwave at full power for 2 minutes followed by 20 minutes at 20% power. After allowing the slides to cool, a border was created with a hydrophobic pen. Slides were washed for 2 min in 1x tris-buffered saline (TBS) wash buffer (1x TBS with 0.05% Tween20), then peroxidase blocked for 15 minutes, followed by 2 more washes (3 min each) with wash buffer. A protein block supplemented with 0.2% Triton X-100 was then performed for 20 minutes after which a 1:100 eIF5B solution in Ab diluent was added for incubation at 4°C for 1 hour. Washing steps were repeated as above followed by a 30-minute incubation with labeled polymer-HRP anti-rabbit reagent. Washing steps were then repeated followed by incubation with (3, 3'-diaminobenzidine (DAB) reagent (1 drop DAB in 1mL DAB substrate for ~5 minutes). Slides were then washed with water for 2 min and then counterstained with hematoxylin for 1 min. Slides were then placed under running lukewarm water for 1 min and then dehydrated by dipping in ethanol solutions of increasing concentration (70%-100%) followed by dipping in 2 separate xylene solutions. After this, slides were fixed with dibutylphthalate polystyrene xylene (DPX) mounting solution and a cover slip was added and left at room temperature overnight. The next day excess DPX was removed and the perimeter of the coverslip was sealed with nail polish and allowed to dry at 4°C. Individual cores were then imaged on the Cytation 5 machine at 10x magnification. Scoring was performed in double-blind based on staining intensity within the cores. A score of 0

was given for no staining, a score of 1 was given for weak staining, a score of 2 was given for medium staining and a score of 3 was given for strong staining as described in [90].

URL for slides used: HN811: https://www.tissuearray.com/p_HN811_2599424852

OR601c: https://www.tissuearray.com/tissue-arrays/Oral_Cavity/OR601c

2.10 Patient Survival Analysis

The patient survival curve for HNSCC was generated using the GEPIA2 database. To generate the figure, Survival Analysis was chosen. eIF5B was listed as the gene symbol and Overall Survival was chosen. A median group cutoff was chosen (50% Cutoff-High(%) and 50% Cutoff-Low(%)). Hazards Ratio (HR) was chosen and the 95% confidence interval as a dotted line was not chosen. The axis units were set as days and HNSC was chosen with the subtype filter, where all subtypes (atypical, basal, classical, and mesenchymal) were chosen for analysis.

2.11 Apoptosis Assay

Cal33 cells were seeded at 1,000 cells/well and reverse-transfected in a 96-well plate. 100 ng/mL TRAIL was added after 92 hours of incubation. 4 hours after TRAIL addition, cells were rinsed in 1x PBS, followed by the addition of 1x annexin binding buffer with 1µg/mL Hoechst as well as Annexin V-FITC. Cells were imaged at 20x magnification using the Cytation 5 plate imager. For visualizing Hoechst and Annexin-V, cells were imaged using a DAPI filter or a GFP filter, respectively.

2.12 Statistical Analyses

Unless specified, all quantified data shows the mean ± standard error of the mean (SEM) for 3 biological replicates. Statistical significance was determined by an unpaired, two-tailed t-test without assuming equal variance. The significance level was set at a p-value of 0.05. Data was analyzed using GraphPad Prism, versions 9-10. A two-tailed t-test was used instead of a one-

tailed t-test as a two-tailed t-test will test if a mean is significantly changing in both directions. Using an α value of 0.05, a two-tailed will assess if the test statistic is in the top 2.5% or bottom 2.5% of a probability distribution. This approach allows us to identify potential changes in the untested direction. An unpaired t-test was chosen over a paired t-test as an unpaired analysis compares independent and unrelated samples. Because we compared variations in cells under eIF5B depletion conditions (or eIF2A or eIF2D depletion) to cells with no proteins depleted, an unpaired analysis was deemed appropriate.

Chapter 3- Results

Results

Oral squamous cell carcinoma (OSCC) is one of the most common cancers globally and despite advances in treatment, the prognosis remains poor with a high recurrence rate [91,92]. OSCC is characterized by dysregulation of the apoptotic and proliferative pathway as well as enhanced invasion and migration [93-95], and resistance to cisplatin, an alkylating agent considered the first-line treatment in the management of OSCC [96-98]. As a result, identifying additional therapeutic targets in the treatment of OSCC is crucial.

To address this clinical challenge, components of mRNA translation machinery are presenting opportunities to identify novel therapeutic opportunities, as the components of protein synthesis machinery have been identified to play a role in various malignancies [99,100]. Translation initiation is a key step in the translation process that can occur via a canonical, cap-dependent manner, but can switch to a non-canonical cap-independent mode of translation initiation when under stress conditions, such as hypoxia or nutrient limitation [73,79,101,102]. Under pathophysiological stress conditions, IRES elements found in the 5' UTR of certain mRNAs can recruit the 40S ribosomal subunit without the need for the 5' cap structure [73,103]. The mRNAs encoding antiapoptotic proteins such as cIAP1, XIAP, Bcl-xL and cFLIPs harbor these IRES elements [31,104-107].

eIF5B has been shown to drive IRES-mediated translation under pathophysiological stress conditions by delivering the initiator tRNA to the P-site of the ribosome [75] and shown to upregulate levels of the antiapoptotic proteins listed above [31]. A body of work has shown that eIF5B expression was associated with resisting apoptotic cell death and its depletion resulted in increased cell death and decreased proliferative and invasive capabilities in cancers such as glioblastoma multiforme (GBM), prostate cancer lung cancer, and hepatocellular carcinoma

[31,86,88,89]. The established role of eIF5B in multiple different malignancies suggests that eIF5B could be playing a role in the survival of OSCC and therefore the overarching objective of my project is to establish the pre-clinical rationale for eIF5B as a therapeutic target in OSCC.

Aim 1: To define the role of eIF5B in OSCC cell survival.

3.1.1 eIF5B expression is correlated with poor patient survival in OSCC

To check if eIF5B is prognostic for HNSCC and OSCC, we performed a bioinformatic analysis of the RNAseq data available through the cancer genome atlas (TCGA). The results indicate that eIF5B gene expression is correlated with poor patient survival (Figure 3.1). Single-cell RNA sequencing (RNA seq, provided by Dr. Pinaki Bose) was performed to analyze the levels of eIF5B mRNA expression in different cell types in OSCC tumor environments (Figure 3.1). Of the different cell types sequenced, the greatest expression of eIF5B mRNA (expressed as black dots) was reported for cancer cells. The wide peak of the box plot high on the y-axis for cancer cells also suggests a high frequency of eIF5B mRNA expression compared to other cell types, suggesting that in OSCC tumors, the high expression of EIF5B is predominantly expressed in cancer cells (Figure 3.1).

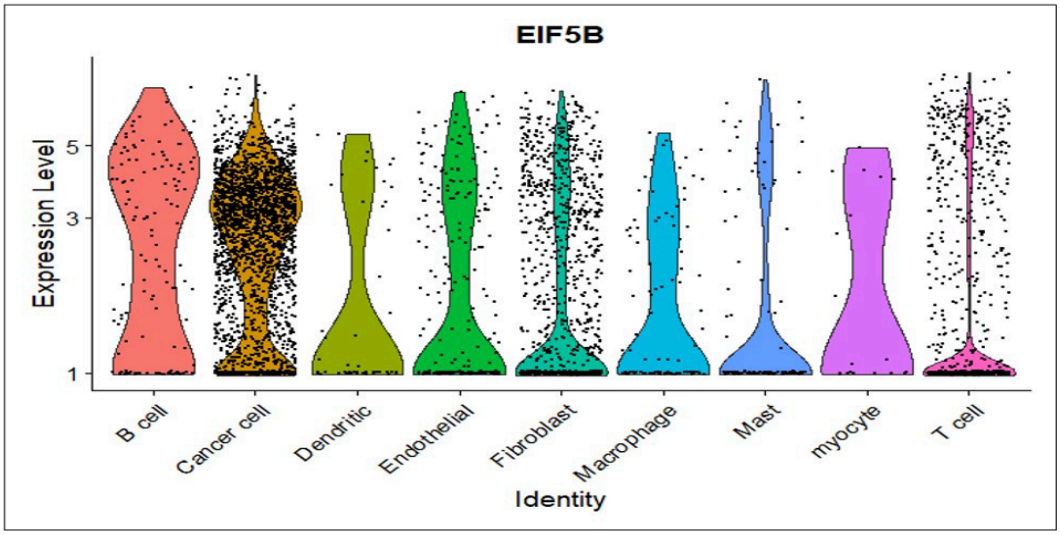

Figure 3.1. EIF5B mRNA expression in OSCC tumors is predominantly located in cancer cells. Single-cell RNA sequencing data was generated and provided by Dr. Pinaki Bose

To visualize the expression of eIF5B protein in OSCC tissue, tissue microarray (TMA) staining was performed (Figure 3.2A-F). To confirm the specificity of staining, TMA staining was first performed in mouse colon tissue with the surrounding muscularis (Figure 3.2A) (data provided by Dr. Bo Young Ahn). eIF5B is highly expressed in colon tissue but poorly expressed in the surrounding muscularis. The staining results reveal strong eIF5B expression (displayed in the brown color) in colon tissue and sparse staining of the muscularis section, suggesting strong specificity of the eIF5B antibody used. Subsequent staining of OSCC tissue (Figure 3.2D-F) compared to cancer-adjacent normal tissues (Figure 3.2B-C) reveals a greater expression of eIF5B in OSCC tissues. Scoring analysis of OSCC (n= 108 cores) and cancer-adjacent normal tissue (n=34 cores) show higher eIF5B protein expression for OSCC tissues compared to cancer-adjacent tissues (Figure 3.2G), suggesting that eIF5B protein is highly expressed in OSCC tissues compared to non-cancerous tissues. The number of cancerous cores compared to non-cancerous cores are unequal because all patients may not have provided cancer adjacent normal tissues. The heterogeneity between cores can be visualized as seen by the unique distribution of staining between cores. Due to the presence of multiple cell types in the tumor environment such as cancer cells or connective tissue, the staining per core is unique due to the heterogeneous nature of the tumors.

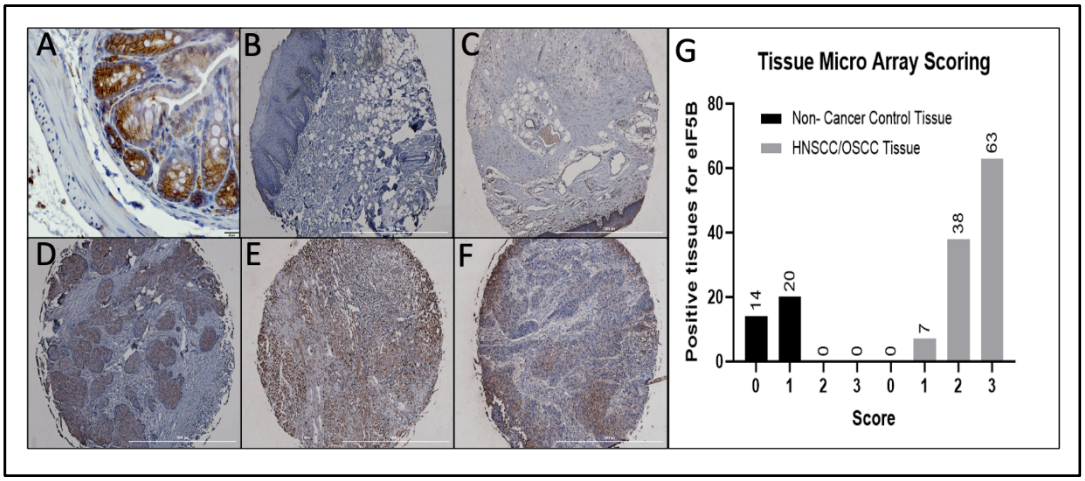

Figure 3.2. eIF5B protein expression is greater in OSCC tissue compared to cancer-adjacent normal tissue. (A) Colon tissue with surrounding muscularis was stained for eIF5B to confirm the specificity of staining. (B-F) OSCC and cancer-adjacent normal tissue cores were de-paraffinized and antigens were activated. Peroxide and protein blocking was performed before incubating with eIF5B primary and secondary antibodies. Slides were then dehydrated and fixed before imaging and scoring. (G) Visual scoring of OSCC TMA slides displaying positive results for eIF5B as a function of tumor score for OSCC and cancer adjacent normal tissues.

Patient survival analyses for head and neck squamous cell carcinoma patients (HNSCC) (Figure 3.3A) and specifically HPV-negative OSCC (Figure 3.3B) reveal that as time progresses, patients with higher-than-median expression of eIF5B have a statistically shorter overall survival probability compared to patients with lower-than-median eIF5B expression (~25% poorer survival probability for higher-than-median eIF5B expression patients after 5000 days).

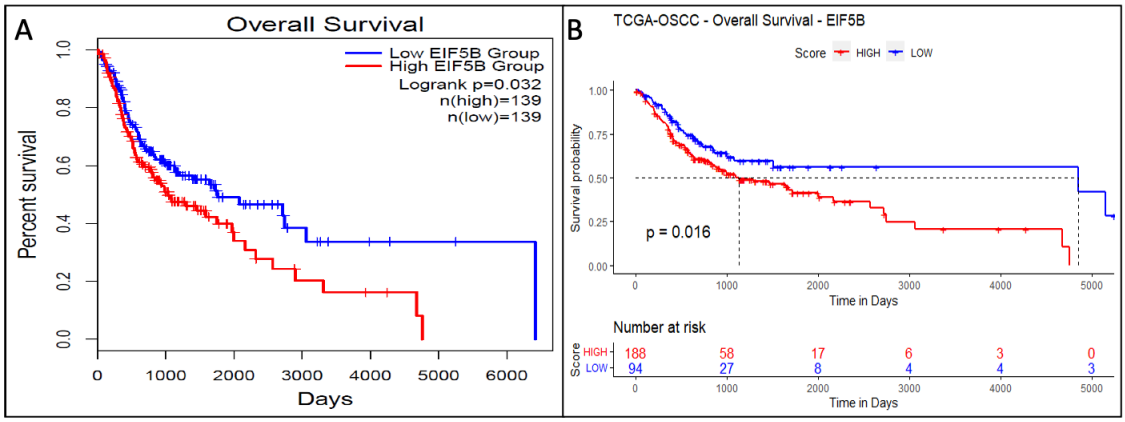

Figure 3.3. EIF5B mRNA transcript expression is correlated with poor patient survival. (A) Patient survival data showing overall survival and eIF5B gene expression in HNSCC patients

was generated using the GEPIA 2 database (B). Patient survival data showing overall survival and eIF5B gene expression in OSCC patients was generated and provided by Dr. Pinaki Bose

3.1.2 eIF5B depletion increased Cal33 cell death with TRAIL treatment

To investigate the impact that depletion of different initiation factors has on the susceptibility of Cal33 cells to TRAIL, alamarBlue assays were performed. Of the initiation factors associated with delivering tRNA in non-canonical conditions studied in this assay, only depletion of eIF5B resulted in a significant reduction in alamarBlue absorbance in the presence of TRAIL compared to eIF5B depletion conditions in the absence of TRAIL (30%) (Figure 3.4).

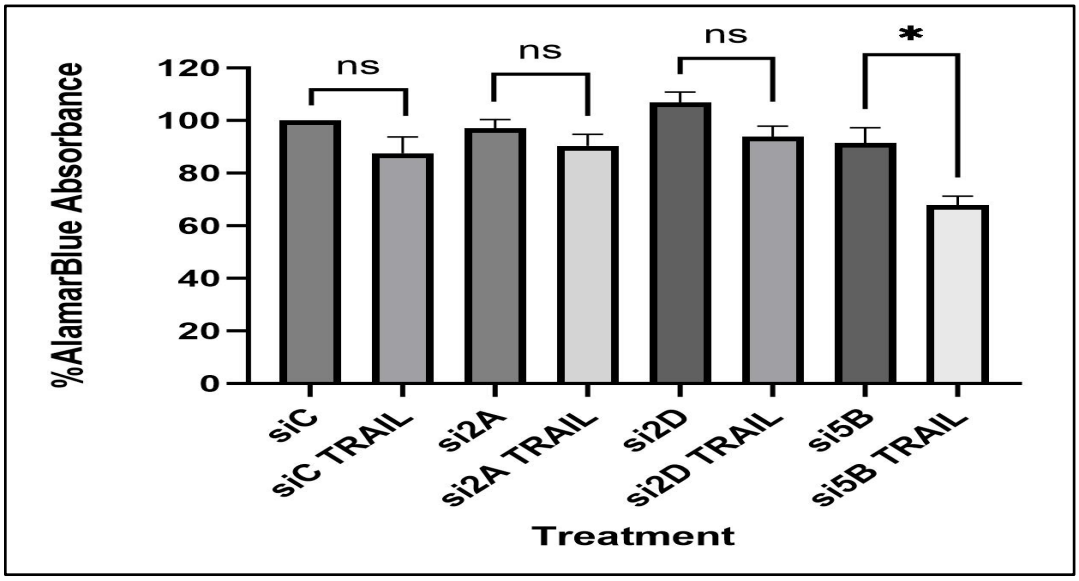

Figure 3.4. eIF5B depletion significantly decreases alamarBlue absorption in Cal33 cells upon TRAIL treatment. Cal33 cells were reverse transfected with a non-specific scrambled control siRNA (siC), or with siRNA specific for eIF2A, eIF2D, and eIF5B (si2A, si2D, and si5B, respectively). 100ng/mL TRAIL was added 48 hours post-transfection. AlamarBlue was added after a further 72 hours followed by a 17-hour incubation with alamarBlue. Data is expressed in mean ± SEM for 3 biological replicates. *, $p < 0.05$

3.1.3 eIF5B depletion reduced levels of anti-apoptotic proteins and activated caspase 7 in Cal33 cells, but not in non-cancerous BJ5TA cells

To assess the effect of eIF5B depletion on cell death of OSCC cells and non-cancerous cells to TRAIL-mediated cell death, cell viability assays were performed using Cal33 and non-cancerous fibroblast BJ5TA cells (Figure 5A and 5B, respectively). There was little change in alamarBlue absorbance between siC and si5B conditions without TRAIL treatment. However, in the presence of TRAIL (an apoptotic agent), eIF5B depletion in Cal33 cells resulted in significantly reduced alamarBlue absorption (40%) compared to si5B conditions without TRAIL or siC conditions with TRAIL (Figure 5A). In cell viability assays performed in BJ5TA cells, there was no significant, or visually noticeable, change in alamarBllue absorption between control or eIF5B depletion conditions, either in the absence or presence of TRAIL (Figure 5B).

To understand why TRAIL treatment had a significant effect on Cal33 cells, I performed western blot analyses of OSCC Cal33 cells and fibroblast BJ5TA under control and eIF5B depletion conditions and measured the levels of the antiapoptotic proteins cIAP1, XIAP, Bcl-xL, $cFLIP_s$ as well as activated/cleaved caspase 7 (Figure 5C-D, respectively). In Cal33 cells, eIF5B depletion resulted in a significant and robust decrease in cIAP1 levels, both in the presence and absence of TRAIL (40% and 60%, respectively); the same trend was seen in Bcl-xL levels as well in Cal33 cells (80% in the absence of TRAIL and 90% in the presence of TRAIL). Levels of $cFLIP_s$ and XIAP were significantly reduced in TRAIL treatment conditions (60% and 40%, respectively) but were not significantly changed in the absence of TRAIL in Cal33 cells. Additionally, under eIF5B depletion and TRAIL conditions, levels of caspase 7 were robustly and significantly increased (200%), suggesting a role of eIF5B depletion in activating the apoptotic pathway under TRAIL treatment.

In contrast, when eIF5B was depleted in BJ5TA cells, there was no significant change in any of the antiapoptotic proteins studied. Caspase 7 was probed for but in all 3 biological

replicates performed, no bands were visible for activated caspase 7. To ensure that cell membrane receptors for TRAIL were present on BJ5TA cells, BJ5TA lysates were subsequently probed for the presence of DR4 and DR5 receptors; the results reveal that these receptors are indeed present in these cells (Figure 5D), suggesting that TRAIL binding would likely does occur in these cells, but the subsequent effect on viability and antiapoptotic proteins seen in the cancerous Cal33 cell line does not take place.

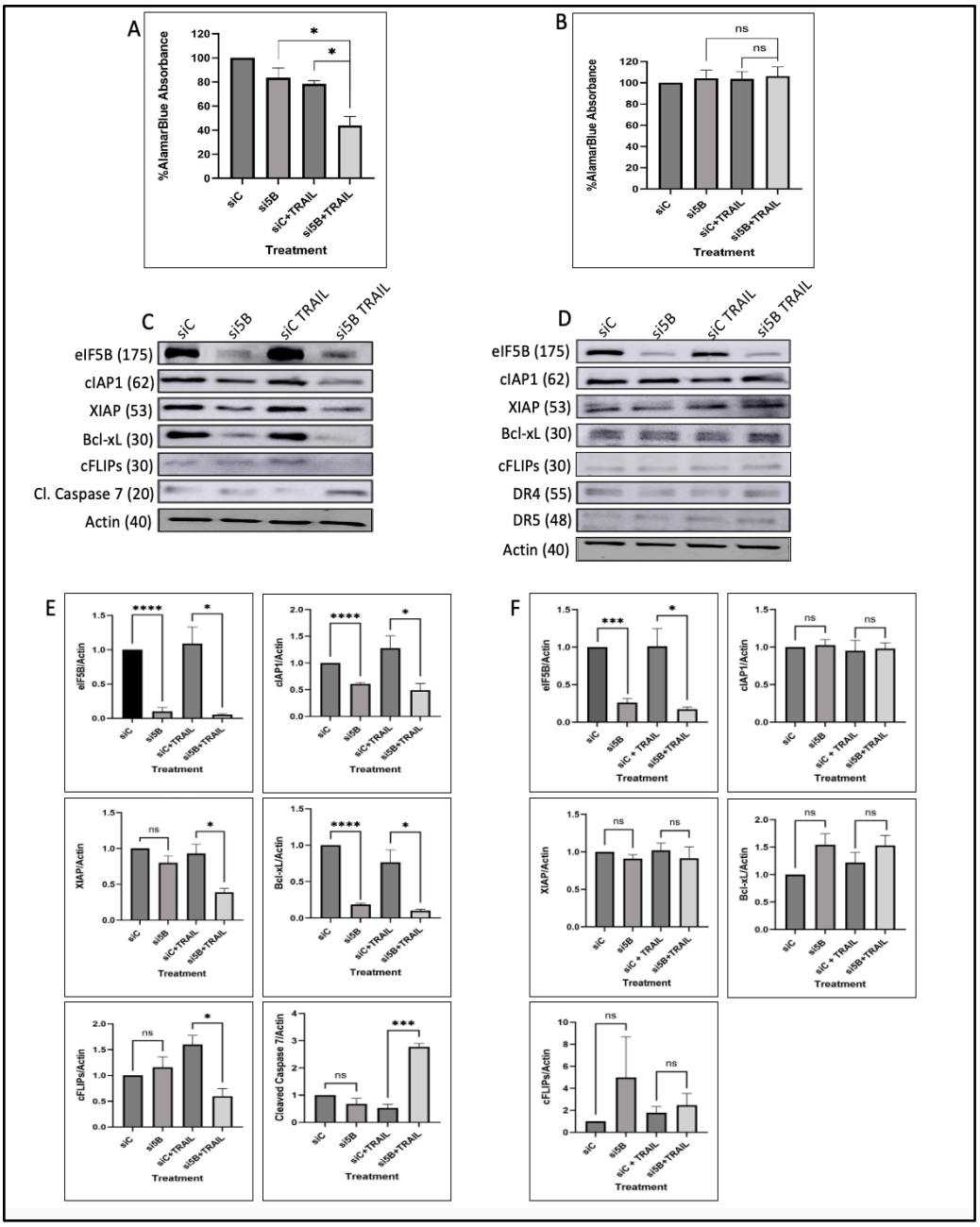

Figure 3.5. eIF5B depletion significantly reduces alamarBlue absorption and levels of antiapoptotic proteins, and activates caspase 7 in Cal33 cells, but not in BJ5TA cells. (A-B) Cell viability data showed significant depletion in alamarBlue absorbance upon eIF5B depletion and TRAIL addition (A), but not in BJ5TA cells (B). Cells were reverse transfected with a non-specific scrambled control siRNA (siC), or with siRNA specific for eIF5B (si5B). 100ng/mL TRAIL was added 48 hours post-transfection. AlamarBlue was added after a further 72 hours followed by a 17-hour incubation with alamarBlue. (C-D). Representative western blot data showing levels of antiapoptotic proteins and activated caspase 7 in Cal33 cells (C) and in BJ5TA (D) in addition to the presence of DR4 and DR5. Cal33 and BJ5TA cells were reverse transfected with a non-specific control siRNA (siC) or siRNA specific for eIF5B (si5B) and incubated for 96

hours. 100ng/mL TRAIL was added 4 hours before harvesting. Cells were harvested in RIPA lysis buffer and 20μg of protein were loaded onto SDS-PAGE for western blotting (40μg for $cFLIP_s$ and caspase 7). (E-F) Quantification of proteins assessed normalized to β-actin. Data is expressed in mean ± SEM for 3 biological replicates. *, $p < 0.05$; **, $p< 0.01$; ***, $p<0.001$; ****, $p<0.0001$

To further visualize the apoptotic process, microscopy images were taken for Cal33 cells under control or eIF5B depletion conditions in the presence or absence of TRAIL. The cells were treated with Hoechst stain and Annexin V-specific stain and visualized in a Cytation 5 plate imager. In one biological replicate assessed, we were able to see the formation of multiple apoptotic bodies under eIF5B depletion conditions in the presence of TRAIL. (as highlighted by arrows in Figure 6). There were no apoptotic bodies detected in any of the other conditions analyzed (siC/si5B without TRAIL, siC in the presence of TRAIL) (Figure 6 A-C). Hoechst staining revealed the presence of nuclear fragmentation when eIF5B was depleted in the presence of TRAIL (Figure 6H); this was not seen in siC or eIF5B depletion conditions in the absence of TRAIL, and nuclear fragmentation was not observed in siC conditions in the presence of TRAIL either (Figure 6 E-G). Annexin V stain suggested phosphatidylserine flipping was occurring at a greater rate in eIf5B depletion and the presence of TRAIL by the presence of cells fluorescing bright green (Figure 6L). Bright green cells can be seen in siC and si5B conditions without TRAIL as well (Figure 6 I-J) but since apoptotic body formation or nuclear fragmentation is not present in these coordinates, these may be artifacts or potentially cells undergoing early steps of apoptosis. As this is a single replicate, statistical significance cannot be stated; however, the microscopy data correlates with the western blot and cell viability data in

Figure 5, further suggesting that eIF5B depletion is enhancing apoptotic cell death in eIF5B-depleted Cal33 cells in the presence of TRAIL.

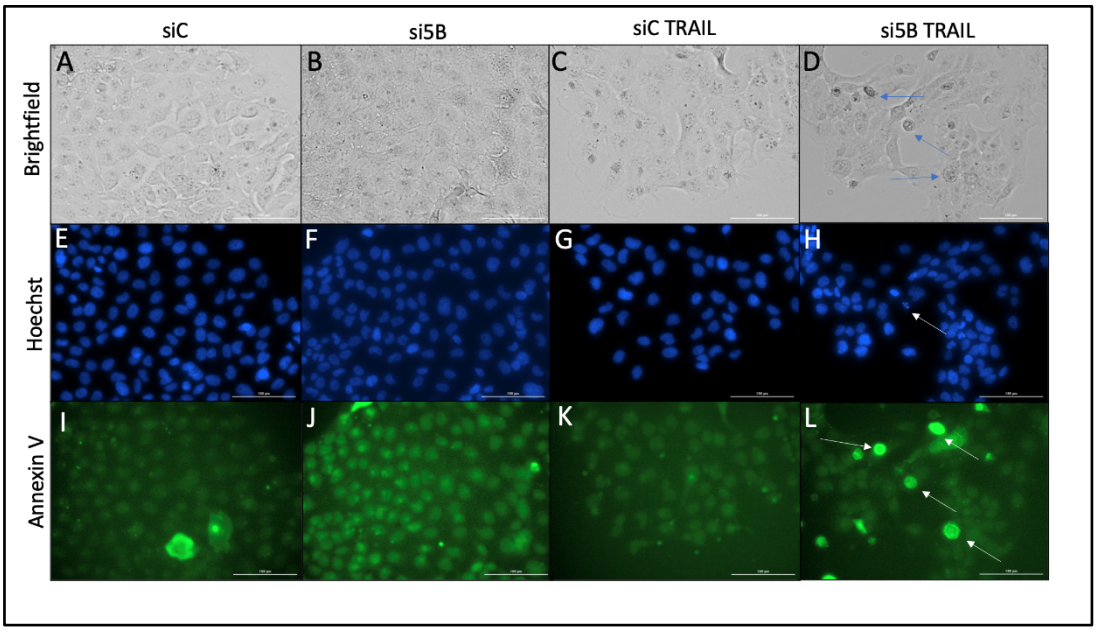

Figure 3.6. Microscopy Images of Cal33 under control or eIF5B depleted conditions in the presence and absence of TRAIL. Cal33 cells were reverse-transfected and incubated for 96 hours. After 92 hours, 100ng/mL TRAIL was added for 4 hours of incubation. Cells were rinsed with 1x PBS and treated with 1x annexin binding buffer with 1µg/mL Hoechst stain as well as Annexin V. A-D: Cells were imaged at 20x magnification by brightfield microscopy. E-H: Cells were imaged at 20x magnification by fluorescence microscopy to analyze Hoechst-stained nuclear DNA or Annexin V-FITC-positive cells (I-L). Brightfield, Hoechst, and Annexin V images for each condition (siC, si5B, siC TRAIL, si5B TRAIL) were taken from the same coordinates.

To summarize, EIF5B mRNA expression is correlated with poor patient outcomes. RNA-seq data revealed that eIF5B is predominantly expressed in cancer cells in the tumor environment and TMA analyses showed that eIF5B expression is higher in OSCC cells compared to cancer-adjacent normal tissues. eIF5B depletion increased cell death in the presence of TRAIL, led to decreased levels of anti-apoptotic proteins and drastically increased activated caspase 7 levels. eIF5B depletion in BJ5TA cells did not affect alamarBlue absorbance in the presence of TRAIL and did not activate caspase 7. Microscopy images revealed the formation of apoptotic bodies, nuclear fragmentation and phosphatidylserine flipping when under eIF5B-depletion conditions in

the presence of TRAIL, phenotypes not detected in the other treatment conditions. These results suggest that eIF5B depletion is enhancing OSCC cell death to apoptotic agents by promoting activation of apoptosis.

Aim 2: To define the role of eIF5B in proliferation, angiogenesis, and invasion and migration of OSCC cells.

In addition to evasion of apoptosis, additional hallmarks of cancer include sustained proliferation, metastasis via invasion and migration and angiogenesis [41,93,108]. Aberrant activity of the MAPK/ERK and NF-κB signalling pathways have been associated with increased proliferation, invasion, and migration phenotypes [51,109]. VEGFA has been reported to be a crucial regulator of angiogenesis [110]. To investigate the impact of eIF5B depletion on the proliferation, invasion, and migration phenotypes of OSCC cells, BrdU incorporation assays, collagen-based invasion assays, and wound healing assays were performed in Cal33 cells, respectively. Cytokine analyses of spent Cal33 media for angiogenic biomarker analyses and endothelial tube formation assays were performed to study the impact of eIF5B depletion on the angiogenic capability of OSCC cells. To see how proteins involved in ERK and NF-κB signalling pathways and angiogenesis are affected upon eIF5B depletion, levels of proteins involved in the MAPK/ERK and NF-κB axes, levels of EGFR, p-EGFR, NF-κB, P-NF-κB, ERK, p-ERK, HIF-1α, and VEGFA were assessed.

3.2.1 eIF5B depletion hinders proliferation, invasion, and migration phenotypes in OSCC cells, but does not hinder proliferation in fibroblast BJ5TA cells

We began by performing BrdU incorporation assays in Cal33 cells to test for changes in proliferation upon eIF5B depletion (Figure 3.7). The results revealed significantly depleted BrdU incorporation upon eIF5B depletion (Figure 3.7A), suggesting hindered proliferative capability

of Cal33 cells. To compare these results to the effects eIF5B depletion would have on BrdU incorporation in a non-cancerous cell line, BrdU incorporation assays were performed in BJ5TA cells (Figure 3.7B). Upon eIF5B depletion, a significant increase in BrdU incorporation was seen, indicating that eIF5B depletion increased the proliferative capabilities of these cells.

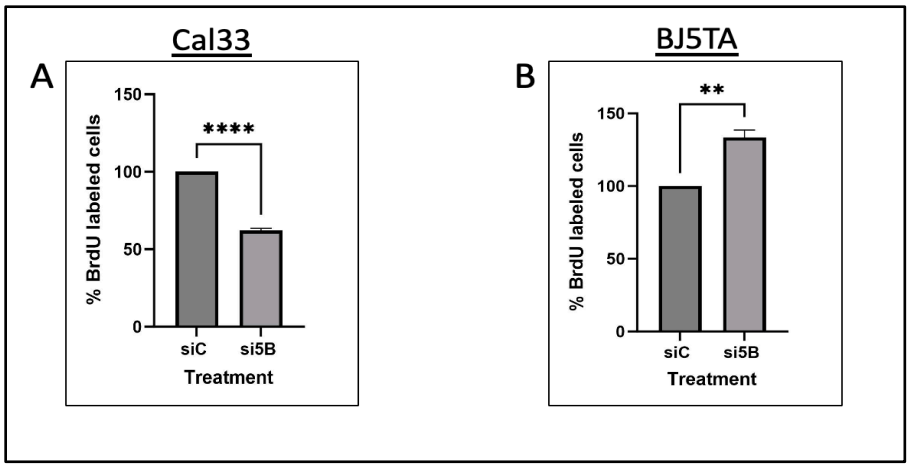

Figure 3.7. eIF5B depletion hinders proliferative and invasive capabilities in Cal33 cells but does not impair proliferation in BJ5TA cells. (A) BrdU incorporation data shows depleted proliferation upon eIF5B depletion in Cal33 cells, but not in BJ5TA cells (B). Cal33 and BJ5TA cells were reverse transfected with a scrambled non-specific control siRNA (siC) or siRNA specific for eIF5B (si5B). 48 hours post-transfection, 1x BrdU was added and incubated for a further 48 hours, after which cells were fixed and incubated with antibodies according to the manufacturer's instructions. Data is expressed in mean ± SEM for 3 biological replicates. **, $p< 0.01$; ****, $p<0.0001$

To assess the effect of eIF5B depletion on the invasive capabilities of Cal33 cells, a collagen layer-based invasion assay was performed (Figure 3.8A). In this assay, Cal33 cells are seeded in serum-free media. Serum-containing media is separated by a collagen layer that is permeable to cells. The invasion of Cal33 cells upon eIF5B depletion through this insert compared to control conditions can indicate how the invasion phenotype is affected. Upon eIF5B depletion, a significant depletion in the percentage of invading cells was seen (32%). After staining, cells that had not invaded through the collagen layer were scraped off and images were taken of the cells that had invaded. Comparing the presence of invaded Cal33 cells as indicated

by the purple stain in the siC condition (Figure 3.8B) compared to eIF5B depletion conditions (Figure 3.8C), there are much fewer cells that have invaded through the collagen layer. These results suggest that eIF5B depletion is hindering the proliferation phenotype in OSCC cells.

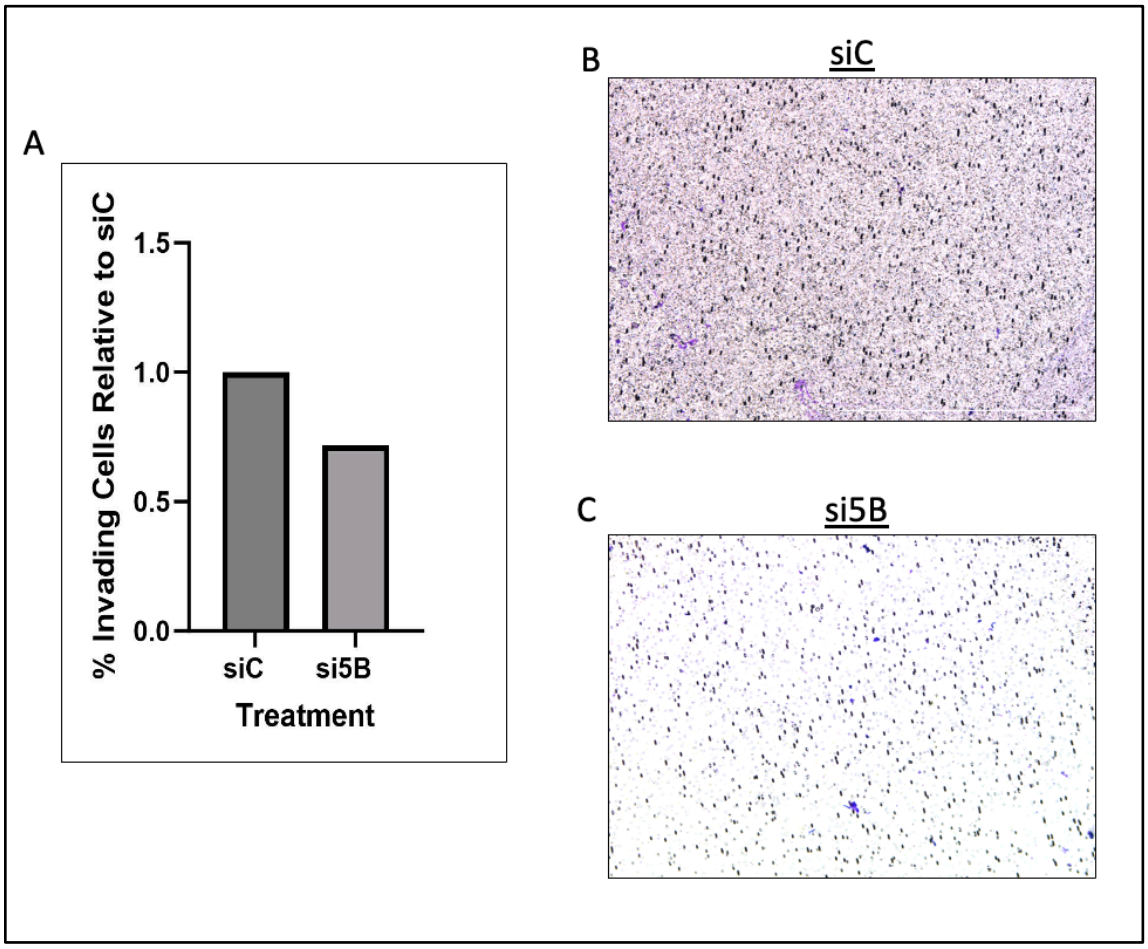

Figure 3.8. eIF5B depletion results in a decrease in OSCC cell invasion. (A) Collagen-based cell invasion assay showed a decrease in the percentage of invading Cal33 cells compared to control conditions. eIF5B depletion reduced the invasive capability of Cal33 cells. Cal33 cells were seeded in serum-free media into collagen inserts and reverse-transfected with either a scrambled control siRNA (siC) or a siRNA specific for eIF5B (si5B). Cells were incubated for 48 further hours to cross the insert into the serum-containing media. Cells were stained and extracted according to the manufacturer's instructions. Upon incubation and staining, non-invaded cells were scraped off and images were taken for Cal33 cells that had invaded the collagen layer under siC treatment (B) or under eIF5B depletion conditions (C).

To investigate the effect eIF5B depletion has on the migratory ability of OSCC cells, wound healing assays were performed in Cal33 cells (Figure 3.9). 24 hours after introducing a

scratch, the results reveal that, in the scrambled control siRNA condition, almost 100% of the scratch area was covered by Cal33 cells. In the eIF5B depletion condition, there was a robust and significant decrease in the wound area covered (65% reduction), suggesting that eIF5B depletion strongly hinders the migratory capability of Cal33 cells.

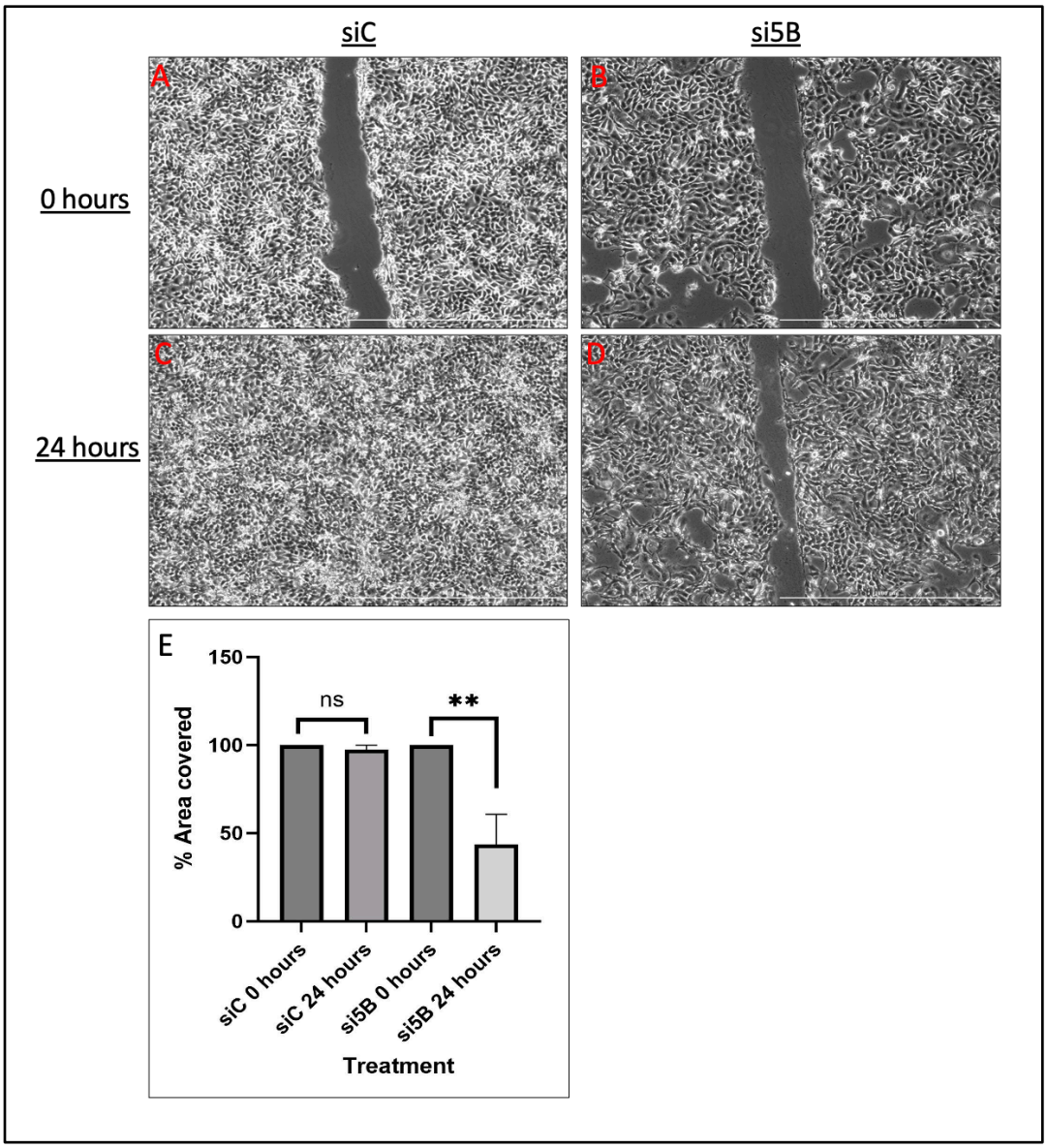

Figure 3.9. eIF5B depletion significantly reduces the migratory capability of Cal33 cells. Cal33 cells were transfected with either a scrambled control siRNA (siC) or siRNA specific for eIF5B (si5B). Upon reaching appropriate confluency, a scratch was introduced with a P10 pipette tip. Brightfield images were taken at the time of scratch introduction and 24 hours after. Wound healing was analyzed using ImageJ software. (A-D) Phase contrast microscopy images showing wound area in siC-treated Cal33 cells at the time of scratch introduction (A), eIF5B depleted

Cal33 cells at the time of scratch introduction, siC-treated Cal33 cells 24 hours after scratch introduction (C) and eIF5B depleted Cal33 cells 24 hours after scratch introduction (D). (E) Quantification of the percentage of wound area covered after 24 hours normalized to wound area at the time of scratch introduction. Data is expressed in mean ± SEM for 3 biological replicates. **, $p < 0.01$. Wound healing assay experiments were performed by Pavan Lakshmi Narasimha

3.2.2 eIF5B depletion reduces the presence of angiogenic markers in spent Cal33 media and hinders certain angiogenic characteristics in HUVEC cells

To assess how levels of angiogenic markers are affected upon eIF5B depletion, Cal33 cells were transfected with a scrambled control siRNA or an siRNA specific for depleting eIF5B. Spent media was collected and sent for a 17-plex discovery assay for angiogenic markers performed by Eve Technologies. Of the markers assessed in the media, significant depletion in VEGF-C, VEGF-A, Endothelin-1, Interleukin 8 (IL-8), and placental growth factor (PLGF) was reported (ranging from 50-80% reduction) (Figure 3.10A-E). It should be noted that the concentrations between the different biomarkers varied drastically, with the highest concentrations being reported for VEGFA (up to 18,000 pg/mL) and the lowest reported concentration being reported for PLGF (up to 1 pg/mL). It may be possible that those factors present in higher concentrations (VEGFA, IL-8) may have a greater impact on angiogenesis compared to those factors present in much lower concentrations. Upon confirmation of reduced angiogenic markers, HUVEC cells were treated with spent media to assess their branching capabilities (Figure 3.10F-G). Upon Image J analysis a significant reduction in the percentages of junctions, segments, and nodes formed (20% reduction) was observed in HUVEC cells (Figure 3.10H-J). The ability to hinder the formation of these in HUVEC cells suggests that eIF5B depletion reduces the angiogenic capability of Cal33 cells.

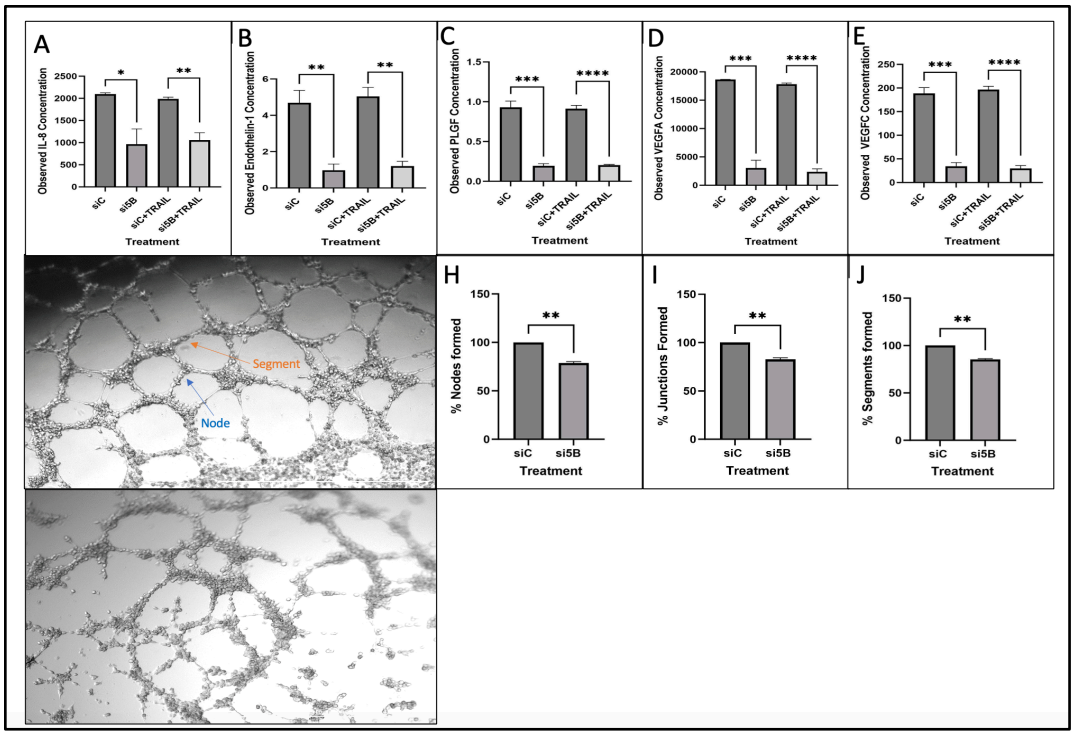

Figure 3.10. eIF5B depletion reduces levels of certain angiogenic markers in Cal33 media and hinders branch formation characteristics in HUVEC cells. (A-E) Levels of angiogenic biomarkers in spent Cal33 media. Cal33 cells were reverse transfected with a non-specific control siRNA (siC) or siRNA specific for eIF5B (si5B) and incubated for 96 hours. 100ng/mL TRAIL was added 4 hours before harvesting. Cells were harvested in RIPA lysis buffer and 20µg of protein were loaded onto SDS-PAGE for western blotting to confirm eIF5B depletion and caspase 7 activation. Spent media was collected after 96 hours of incubation and centrifuged at 3,000 rpm for 2 minutes. 200µL were aliquoted and stored for angiogenic marker analysis by Eve Technologies. The concentrations provided are in pg/mL. (F-G) Representative images of HUVEC branch formation. HUVEC cells were seeded into a Matrigel matrix in HUVEC-specific media before being supplemented with spent Cal33 media treated with either a scrambled control siRNA (siC) or siRNA specific for eIF5B (si5B). Branch formation was allowed to take place for 6 hours before images were taken. (H-J) Quantification of percentages of junctions, segments, and nodes formed in control and eIF5B depletion conditions. Quantifications were performed using the ImageJ angiogenesis macro program. (A-E) Data is expressed in mean ± SEM for 3 biological replicates. (H-J) Data is expressed in mean ± SEM for 2 biological replicates. *, $p < 0.05$; **, $p< 0.01$; ***, $p<0.001$; ****, $p<0.0001$

3.2.3 eIF5B depletion reduces levels of HIF-1a and VEGF in Cal33 cells and hinders proliferative, invasive, and migratory capabilities of Cal33 cells, but does not hinder proliferation in BJ5TA cells.

To study the effect of eIF5B depletion on known drivers of invasion, migration, and proliferation, western blot analyses were performed. Cal33 cells were treated with a scrambled control siRNA or with an eIF5B-specific siRNA to deplete eIF5B in the presence and absence of TRAIL. Levels of HIF-1α, EGFR, phosphorylated EGFR (P-EGFR), NFκB, phosphorylated NFκB (P-NFκB), ERK, phosphorylated ERK (P-ERK), and vascular endothelial growth factor A (VEGFA) were assessed in one biological replicate (Figure 3.11A). Upon eIF5B depletion, there was a robust decrease in HIF-1α in the absence and presence of TRAIL (75% and 85%, respectively, Figure 11C). There was also a noticeable decrease in HIF-1α in the scrambled control with TRAIL (40%). A similar pattern of depletion was seen for VEGFA (Figure 3.11J) and p-ERK levels (Figure 3.11I). Analysis of EGFR reveals an increase in EGFR levels upon eIF5B depletion (40%, Figure 11D) in the absence of TRAIL, but a decrease was reported in the presence of TRAIL (40%). p-EGFR levels decreased upon eIF5B depletion in the absence and presence of TRAIL (50% and 25%, respectively; Figure 11E); p-EGFR levels also decreased about 50% in the scrambled control condition upon TRAIL treatment (Figure 3.11F). NF-κB levels were noticeably reduced upon eIF5B depletion in the presence of TRAIL (50%); a decrease in NF-κB was also observed in the scrambled control condition with TRAIL (35%). A similar robust depletion in p-NF-κB was observed upon eIF5B depletion with TRAIL treatment (75%, Figure 11G). p-NF-κB levels were also decreased upon eIF5B depletion in the absence of TRAIL and scrambled control condition in the presence of TRAIL (40%). Analysis of ERK revealed a strong depletion upon eIF5B depletion in the presence of TRAIL (75%, Figure 11H). To summarize, a single replicate analysis showed that eIF5B depletion resulted in the depletion of multiple proteins known to be involved in proliferative, migratory, and invasion pathways, especially HIF-1α, VEGF, p-NF-κB and p-ERK.

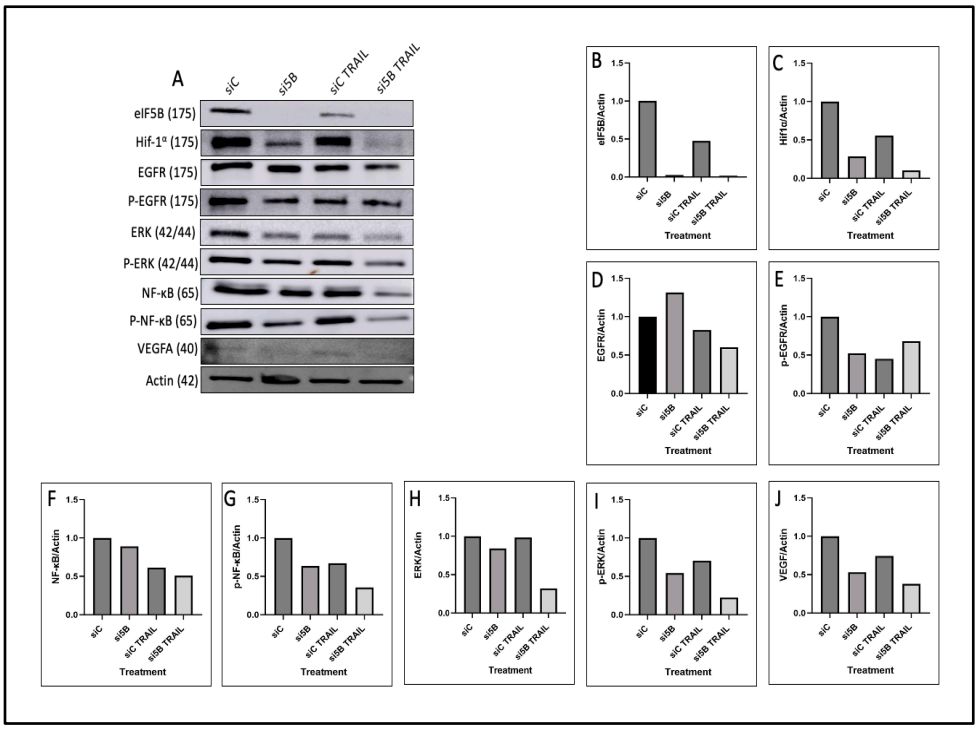

Figure 3.11. eIF5B depletion decreases levels of known drivers of proliferation, invasion and migration. (A) Western blot data showing levels of eIF5B and proteins involved in proliferation, migration and invasion pathways. Cal33 cells were reverse transfected with a non-specific control siRNA (siC) or siRNA specific for eIF5B (si5B) and incubated for 96 hours. 100ng/mL TRAIL was added 4 hours before harvesting. Cells were harvested in RIPA lysis buffer and 20µg of protein were loaded onto SDS-PAGE for western blotting. (B-J) Quantification of proteins assessed normalized to β-actin.

Aim 3: To establish the pipeline (validate reagents) for studying the role of eIF5B in OSCC using an orthotopic xenograft mouse model

3.3.1 eIF5B can be successfully depleted using shRNA, which decreased the viability of Cal33 cells to cisplatin

To transition experiments into in vivo orthotopic xenograft mouse model work, eIF5B depletion must be established with the use of short hairpin RNAs (shRNAs). Upon optimization of the use of shRNA to deplete eIF5B levels in Cal33 cells, robust, significant, and sustained eIF5B depletion was seen for the initial transduction and 2 subsequent passages (65% for the initial transduction and 80% for the 2 subsequent passages) (Figure 3.12A-B). To investigate the impact eIF5B depletion would have on Cal33 cell death to cisplatin, a kill curve for cisplatin was first generated. An IC_{50} value of 19.42 μM was obtained (Figure 3.12C); as a result, subsequent experiments were performed with a 20 μM cisplatin concentration. Cell viability analyses revealed a drastic and significant reduction in alamarBlue absorbance upon eIF5B depletion and treatment with cisplatin (80% reduction, Figure 12D). Invasion assays using shRNA were performed and the results indicate shRNA-mediated eIF5B depletion also significantly impaired invasive capabilities in Cal33 cells (50%, Figure 12E).

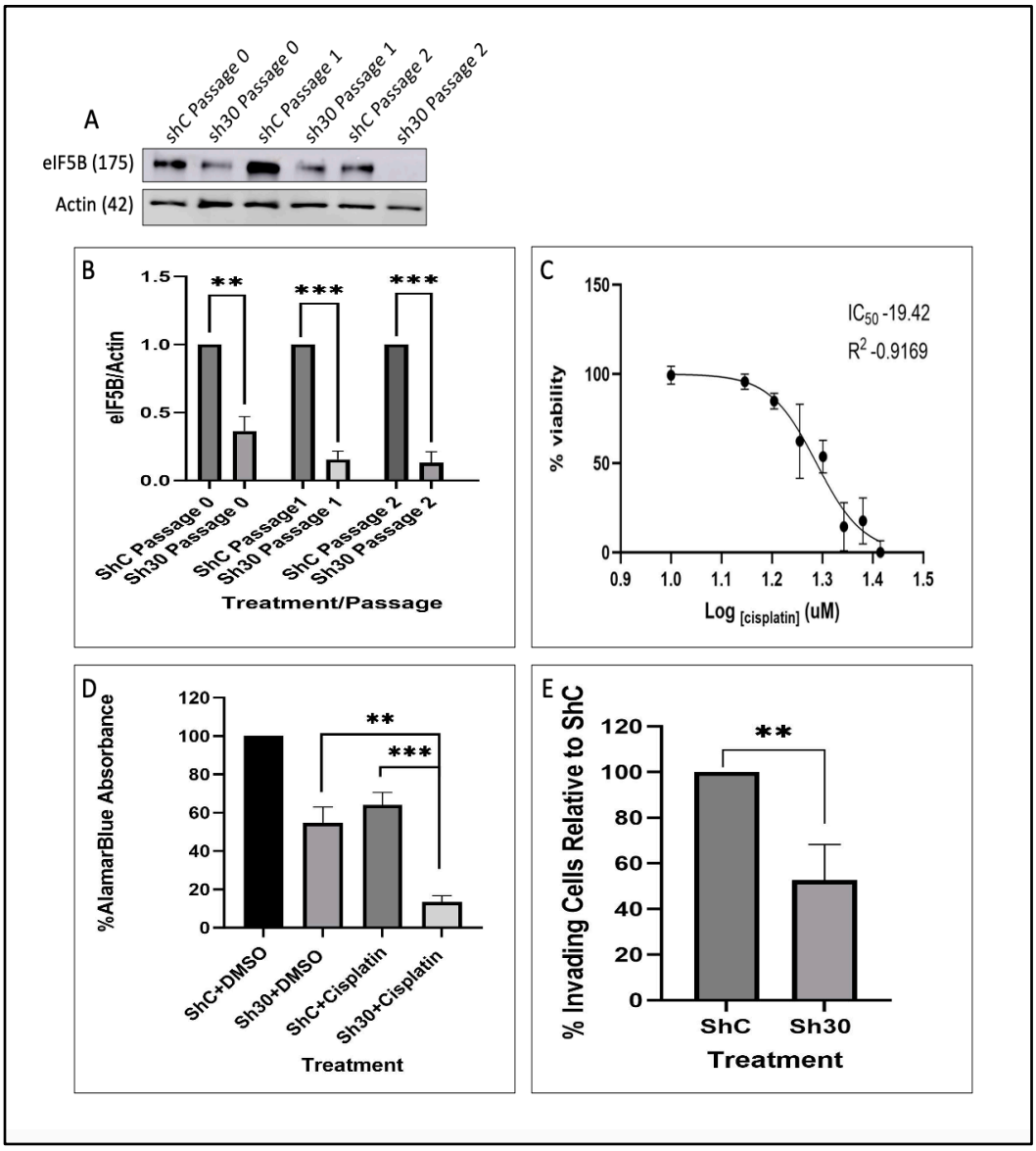

Figure 3.12. eIF5B is successfully depleted using shRNA in Cal33 cells and eIF5B depletion increases Cal33 cell death in the presence of cisplatin and hinders invasive capabilities. A: eIF5B depletion with shRNA lasts multiple passages. Cal33 cells were transduced with either a scrambled control shRNA (shC) or shRNA specific for eIF5B (sh30) and seeded in media supplemented with 2μg/mL puromycin. After selection, half of the wells were harvested, generating Passage 0 and half of the wells were seeded again (Passage 1). This process was repeated once again, generating passage 2. B: Quantification of eIF5B through multiple passages normalized to β-actin. C: Cal33 kill curve for cisplatin revealed an IC_{50} value of 19.42μM. Cal33 cells were transduced as described above and subsequently seeded into a 96-well plate. 24 hours after seeding, different cisplatin was added, ranging from 0-30μM. After a further 72 hours, alamarBlue was added and absorbance readings were taken 17 hours after. D: eIF5B depletion increased Cal33 cell death to cisplatin. Cal33 cells were transduced and subsequently seeded as described above. 24 hours after seeding, 20μM cisplatin was added. After a further 72 hours, alamarBlue was added and absorbance readings were taken 17 hours after. E: eIF5B depletion

reduces the invasive capability of Cal33 cells. Transduced and puromycin-selected cells were seeded in serum-free media into a collagen insert with serum-containing media on the other side of the insert. Cells were incubated for 48 hours and stained and extracted according to the manufacturer's instructions. Western blotting, cell viability, and invasion assay data are expressed in mean ± SEM for 3 biological replicates. *, $p < 0.05$; **, $p< 0.01$; ***, $p<0.001$; ****, $p<0.0001$

Chapter 4- Discussion and Future Directions

Discussion

OSCC is an aggressive cancer with a high mortality rate and unfavourable patient prognosis despite improvements in treatments [5,111,112]. Therefore, additional therapeutic opportunities must be explored. In this work, I investigated the potential of eIF5B as a therapeutic for OSCC. First, I aimed to define the role of eIF5B in OSCC cell survival. I then wanted to study the role of eIF5B in the proliferation, invasion, migration, and angiogenesis of OSCC cells. Finally, to generate the reagents for experiments in an orthotopic xenograft mouse model, I wanted to establish stable shRNA-mediated knockdown of eIF5B in OSCC cells and test their cell viability under the treatment of cisplatin.

To establish a link between EIF5B mRNA expression and poor patient outcomes, I performed a bioinformatic analysis of publicly available RNAseq data. The single-cell RNAseq data demonstrated that EIF5B mRNA expression was found to be expressed predominantly in cancer cells in OSCC tumors (Figure 1), compared to other cells within the tumor microenvironment. eIF5B protein expression was higher in OSCC tumor cores compared to cancer-adjacent normal tissue (Figure 3.2). Additionally, patient survival analyses performed by Kaplan-Meier plots revealed a significant decrease in overall survival for patients with high EIF5B mRNA expression (Figure 3.3). This data suggests that EIF5B mRNA level is prognostic for OSCC tumors and intrigued me to investigate if eIF5B can be established as the therapeutic target for OSCC treatment. Under cellular stress conditions, the switch from canonical cap-dependent to non-canonical cap-independent translation initiation has been well established [31,75,76,113]. Under certain stress conditions, the selective translation of mRNAs harboring IRES elements is regulated by eIF5B [75]. Distinct anti-apoptotic proteins such as cIAP1, XIAP, Bcl-xL, and $cFLIP_s$ are translated using IRES elements [31,104-107], and eIF5B has been reported to regulate

the translation of these mRNAs [31]. Thereby, eIF5B can provide critical survival advantages to the cells under pathophysiological stress conditions. As eIF5B is crucial for regulating the translation of mRNAs encoding distinct anti-apoptotic proteins [31], OSCC tumors with high eIF5B expression will likely result in higher levels of antiapoptotic proteins being translated, enabling increased survival and proliferation of these tumor cells. As mentioned earlier in this thesis, eIF5B regulates IRES-mediated translation initiation by regulating the initiator tRNA delivery to the ribosome [75]. Like eIF5B, among the regulators of mRNA translation, eIF2A and eIF2D are also reported to interact with initiator tRNA and take part in IRES-mediated translation initiation [114]. However, depletion of eIF2A or eIF2D did not increase the cell death of OSCC cells under TRAIL treatment conditions (Figure 3.4). In contrast, eIF5B depletion resulted in increased cell death of OSCC cells under TRAIL treatment conditions (Figure 3.4). This suggests that eIF5B is unique among the regulators of non-canonical translation and can be implicated in the OSCC pathophysiology.

The significant increase in the TRAIL-mediated cell death upon eIF5B depletion in combination with the decreased levels of antiapoptotic proteins (Figure 3.5) further supports the role of eIF5B in the survival of OSCC cells likely via regulating the translation of mRNAs encoding antiapoptotic proteins. This could be due to the translational regulation of mRNAs encoding distinct anti-apoptotic proteins, however, to confirm that polysome profiling experiments will need to be performed to establish this notion. eIF5B depletion alone (without TRAIL treatment) or the control cells treated with TRAIL did not affect viability to the extent of eIF5B depletion with TRAIL treatment. The drastic increase in the levels of cleaved caspase 7 when eIF5B is depleted in the presence of TRAIL, not seen in any of the other conditions (siC

and eIF5B depletion in the absence of TRAIL and siC in the presence of TRAIL), suggests activation of the apoptotic pathway. Comparing this to the effects of eIF5B depletion in fibroblast BJ5TA cells, we can see no significant change in viability or levels of antiapoptotic proteins. Since antiapoptotic proteins did not decrease upon eIF5B depletion, I did not see a phenotypic effect under eIF5B depletion in BJ5TA cells.

Microscopy images of Cal33 cells revealed the formation of apoptotic bodies (Figure 6D), nuclear fragmentation (Figure 6H), and phosphatidylserine flipping under eIF5B depletion conditions in the presence of TRAIL (Figure 6L). In healthy cells, the lipid composition of the cell membrane is asymmetrical [115]. Under these conditions, phosphatidylserine is a phospholipid predominantly localized in the inner membrane with its polar head exposed to the cytoplasm [115]. During apoptosis, this asymmetry is lost and enzyme-mediated "flipping" of phosphatidyl serine to the outer lipid bilayer can occur [115,116]. Annexin V is a calcium-binding protein that can bind to phosphatidylserine [115] and fluorescently labelled annexin V can be used to detect this event as cells appear bright green. Another indicator of apoptosis is the fragmentation of DNA, which can be identified by the binding of a DNA-specific stain, such as Hoechst 33342, which can stain DNA in live cells and be visualized with fluorescent microscopy [117,118]. Additionally, apoptosis results in loss of cell adhesion and abnormal membrane appearance [119] which can be visualized using brightfield microscopy. No apparent apoptotic body formation, nucleotide fragmentation or phosphatidylserine flipping was detected in the control or eIF5B depletion without TRAIL or control conditions in the presence of TRAIL (Figure 3.6). There is a bright signal for annexin V staining for siC conditions (Figure 3.6I). Since there is no apoptotic body formation or nuclear fragmentation present in these coordinates, the bright signal may likely be an artifacts. In

summary, eIF5B depletion seems to activate the apoptotic pathway in OSCC cells, thus increasing cell death to pro-apoptotic agents such as TRAIL. The effects of eIF5B depletion in BJ5TA cells seem to suggest that the levels of antiapoptotic proteins are not decreased. Some reports suggest depletion of eIF5B from HEK 293T cells or WI38 cells does not reduce the levels of distinct anti-apoptotic proteins [31,76] under normal growth conditions. These reports corroborate my findings in BT5TA cells (non-cancer cells) and suggest that the eIF5B depletion effect on anti-apoptotic proteins is largely restricted to cancer cells.

As mentioned earlier, characteristic hallmarks of cancer also include phenotypes such as uncontrolled proliferation, metastasis via invasion and migration, and angiogenesis [39,40]. To explore the role of eIF5B in the proliferation of OSCC cells, we performed 5-bromo-2'-deoxyuridine (BrdU) incorporation assays in Cal33 and BJ5TA cells. BrdU is a thymidine analog that incorporates into newly synthesized DNA; BrdU incorporation can hence be measured by immunostaining of fixed cells [120]. Since the concentration of BrdU incorporation can be correlated with new DNA synthesis, a decrease in BrdU incorporation can be associated with decreased proliferation. Upon eIF5B depletion in Cal33 cells, a significant depletion in BrdU incorporation was reported, suggesting that eIF5B depletion hinders proliferation capability in OSCC cells. Interestingly, BrdU incorporation was significantly increased in BJ5TA cells upon eIF5B depletion, which indicates that in these non-cancerous cells, depletion of eIF5B is increasing proliferation.

Metastasis has been identified as a major cause of failed treatments and cancer-associated deaths [121]. Metastasis is the process by which cancer cells grow in distant sites [122]. Key steps in

the initial processes of metastasis are the migration of cancer cells from the original site and invasion through surrounding tissues, into blood and/or lymph vessels and invasion through tissues at distal sites [40,108]. We performed collagen-based invasion assays and wound migration assays to assess invasion (Figure 3.8) and migration phenotypes (Figure 3.9) in OSCC cells, respectively. In Cal33 cells, a decrease in OSCC cell invasion was also detected. Additionally, wound healing assays also suggest depleted migratory capabilities in Cal33 cells.

Two cellular signalling pathways involved in promoting proliferation, invasion, and migration in cancer cells are the NF-κB and MAPK/ERK pathways [48,123,124]. To assess how these phenotypic changes occur upon eI5B depletion, I performed a western blot analysis and determined the levels of protein markers involved in these axes. We looked at changes in EGFR, p-EGFR, NF-κB, p-NF-κB, ERK, p-ERK, VEGF, and HIF-1α upon eIF5B depletion. In one replicate of western blotting, there was a noticeable decrease in levels of HIF-1α, p-EGFR, p-NF-κB, p-ERK, and VEGFA upon eIF5B depletion (Figure 3.11). Similar decreases were also seen under siC conditions with TRAIL. Except for p-EGFR, the most robust decrease in these proteins was detected under eIF5B depletion in the presence of TRAIL. For unphosphorylated EGFR, NF-κB and ERK, their respective levels were not drastically impacted upon eIF5B depletion alone; a noticeable decrease in NF-κB was also seen in siC conditions under TRAIL treatment. For all these proteins, the most noticeable decrease was also seen for eIF5B depletion conditions with TRAIL treatment, with the most robust decrease being seen for ERK. These results suggest a possible route for how OSCC cell proliferation, invasion, and migration were affected upon eIF5B depletion.

The MAPK/ERK pathway begins with the binding of a growth factor or mitogen to a receptor, resulting in its phosphorylation/activation [125]. EGFR has been identified as having a pivotal role in activating ERK signalling and has been implicated in abnormal proliferation in numerous cancers [126,127]. This leads to a phosphorylation (and subsequent activation) cascade, ultimately leading to the phosphorylation/activation of ERK1/2 which translocates to the nucleus to activate transcription factors [128] (eg, ribosomal S6 kinases (RSK1-4) which have been reported to regulate proliferation, invasion, and migration [52] and implicated in OSCC growth [3]. EGFR activation can also lead to activation of the MAPK signalling, which consists of serine-threonine kinases that are regulated via phosphorylation and have been implicated in metastasis in different tumors [129]. EGFR mRNA has been reported to contain [130]. Thus, the decrease in p-EGFR upon eIF5B depletion suggests that eIF5B may be regulating levels of EGFR via IRES elements. Since eIF5B depletion resulted in a drastic decrease in the levels of p-ERK, this may lead to decreased activation of these transcription factors, leading to the decreased proliferation, invasion, and migration witnessed in OSCC cells. VEGFA expression has been reported to activate the ERK pathway in gliomas; thus, the decrease in VEGFA levels upon eIF5B depletion may reduce the level of ERK pathway activation, aiding in decreased proliferation, invasion and migration phenotypes [65].

It was interesting to see the expression of HIF-1α in Cal33 cells even though they were not subjected to hypoxic conditions as HIF-1α is synthesized but rapidly degraded under normoxic conditions [131] . HIF-1α under normoxic conditions was detected in neuroblastoma cells where it was suggested to have a metabolic role in processes needed for tumor cell viability [55]. It has been observed that HIF-1α stabilization can occur under normoxic conditions by the inflammatory regulators Interleukin-8 (IL-8) and macrophage colony-stimulating factor (M-CSF)

followed by translocation to the nucleus to promote transcription HIF-1α-related genes (M-CSF) [132]. The decrease in the levels of these proteins upon eIF5B depletion indicates that eIF5B may be involved in the regulation of key proteins involved in proliferation, invasion and migration. It is reported that hypoxia is present in early tumor development and HIF-1α is important in helping cancer cells adapt to these conditions [43,54]. The decrease in HIF-1α levels seen upon eIF5B depletion suggests that eIF5B depletion in tumors may make tumors less adaptable to hypoxia and may help in stopping tumor development and growth. To summarize, the depletion of eIF5B in OSCC cells resulted in decreased proliferation, invasion, and migration. Western blot analyses showed that known markers of these processes were decreased upon eIF5B depletion, suggesting that eIF5B depletion may hinder these phenotypes by downregulating the activity of the ERK and NF-κB pathways. The decrease in HIF-1α levels upon eIF5B depletion suggests that eIF5B depletion may hinder tumor growth and development by making tumors less adaptable to hypoxic conditions.

The NF-κB pathway can occur through a canonical or non-canonical pathway [133]. The canonical pathway is activated by a diverse array of ligands; this pathway leads to degradation of the NF-κB inhibitor IκBα, allowing the NF-κB components p50 and RelA(p65) to translocate to the nucleus to regulate transcription of target genes [134,135]. The non-canonical pathway is specifically activated by ligands of the tumor necrosis factor receptor (TNFR) superfamily; this pathway does not include IκBα degradation but the processing of a protein called p100, resulting in p52 formation; the p52/RelB dimer then translocates to the nucleus [134]. Canonical NF-κB signaling is involved in most aspects of immune responses whereas non-canonical activation seems to aid in specific adaptive immune responses [134]. NF-κB signalling is involved in immune

responses and inflammation [62]. Aberrant NF-kB activity has been associated with cancer progression by compromising the immune system from attacking tumor cells and inducing cell proliferation [62]. Upon eIF5B depletion, levels of NF-κB were not drastically affected; levels of NF-κB were decreased by 40% under siC conditions with TRAIL and 50% with eIF5B depletion with TRAIL treatment. Levels of p-NF-κB decreased by 40% under the eIF5B depletion condition in the absence of TRAIL and siC conditions in the presence of TRAIL. A robust decrease (70%) was seen for eIF5B depletion conditions in the presence of TRAIL. Constitutive activation and aberrant activity of the NF-κB pathway has been linked with pro-tumorigenic effects such as increased proliferation and malignant cell invasion and migration [109,136]. Therefore, the decrease in p-NF-κB seen under eIF5B depletion suggests that eIF5B depletion may also be impacting the proliferative phenotype observed by regulation of NF-κB signalling.

There is a body of work suggesting that crosstalk EGFR/ERK and NF-κB pathways, HIF-1α and VEGF can contribute to proliferation, invasion, and angiogenesis phenotypes while suppressing apoptosis. EGFR activation by epidermal growth factor (EGF) was linked to NF-κB signalling activation by multiple mechanisms, such as inducing phosphorylation of the NF-κB inhibitor IKKB [137]. Additionally, activated NF-κB promotes transcription of the KIAA1199 gene, which cycles back to EGFR signalling by promoting EGFR phosphorylation and epithelial-mesenchymal transition (EMT) in cervical cancer cells, suggesting how these pathways combine to sustain cell survival and invasion [137]. In pancreatic cancer cells, activation of the EGFR/MEK/ERK pathway leads to increased HIF-1α expression, which limits the excessive release of reactive oxygen species (ROS) and this reduction of ROS activates EGFR in a positive feedback loop to aid in invasion and subsequent metastasis [138].

Cytokine assays of spent OSCC cell media under control and eIF5B depletion conditions were performed in the presence and absence of TRAIL. Under eIF5B depletion conditions, significant reductions in the levels of the angiogenic biomarkers IL-8, Endothelin-1, PLGF, VEGFA, and VEGFC were detected (Figure 3.10). IL-8 has been reported to increase endothelial cell tube formation by directly interacting with endothelial cells and increasing mRNA levels of VEGFA [139,140]. In chondrosarcoma cells, Endothelin-1 promoted the growth of vascular endothelial tissue to facilitate angiogenesis and metastasis [141]. PLGF has been shown to direct VEGF to a VEGF receptor to promote angiogenesis [142]. VEGFA and VEGFC are members of the VEGF family that promote angiogenesis by binding to VEGF receptors and triggering signalling cascades that promote endothelial cell proliferation and migration by increasing the permeability of existing vessels [143]. The decrease in the levels of these markers upon eIF5B depletion suggests that eIF5B depletion in OSCC cells may have the potential to hinder angiogenesis. When HUVEC cells were treated with spent Cal33 media from cells under siC or eIF5B depletion conditions, a significant reduction (20%) was seen in the percentage of nodes, junctions, and segments formed in HUVEC cells under eIF5B depletion conditions. These parameters have been used in literature as a measure of HUVEC growth and correlated with angiogenic potential [144]. Therefore, eIF5B depletion may hinder the angiogenic capabilities of OSCC cells.

In addition to the role of VEGF and the biomarkers listed above, HIF-1α has also been reported to be a master regulator of angiogenesis by interacting synergistically with other angiogenic biomarkers, including VEGF [145]. As discussed above, HIF-1α and VEGF have also been linked to proliferation, invasion, and migration. Interestingly, both VEGF and HIF-1α mRNAs are known to harbour IRES elements [83,84]. As eIF5B has been known to regulate IRES-mediate translation, eIF5B may be likely to be involved in these processes affecting oncogenesis.

Transfection of OSCC cells for experiments in vitro is quick and efficient; however, they have some disadvantages when working with animal models. siRNA-mediated knockdown of eIF5B is only stable for one passage; however, with the use of shRNA-mediated knockdown, stable eIF5B knockdown can be maintained over multiple passages. A report suggests that the use of shRNA was found to be less likely to initiate an inflammatory response compared to siRNA of the same sequence, likely because shRNA is spliced by the cell's own mechanisms [146]. Therefore, we aimed to establish shRNA-mediated knockdown of eIF5B in Cal33 cells to transition experiments into orthotopic xenograft mouse model work. We were able to see stable eIF5B depletion using shRNAs lasting for the initial transduction and two subsequent passages (Figure 3.12 A-B). Using shRNA-mediated knockdown of eIF5B, cell viability assays were performed with cisplatin, the front-line therapeutic for OSCC treatment [96]. Under eIF5B depletion conditions with DMSO or control conditions with cisplatin, there was a 40-50% reduction in alamarBlue absorbance. The most robust decrease in alamarBlue absorbance was seen under eIF5B depletion and cisplatin treatments (80% reduction) (Figure 3.12 D). Because cisplatin is an alkylating agent that induces DNA damage, this stressor may lead to the unfolded protein response [147], leading to eventual phosphorylation of eIF2α and reliance upon IRES-mediated translation. These results suggest that successful and stable eIF5B depletion may be achieved in mouse models and that there may be increased OSCC cell death in mice with eIF5B depleted conditions to cisplatin. Additionally, shRNA-mediated knockdown of eIF5B in OSCC cells resulted in decreased invasion compared to control conditions (Figure 3.12E), suggesting that eIF5B-depleted OSCC cells in mouse models may exhibit decreased invasive capabilities. Given the influence of eIF5B reported in this project, identifying/generating drugs that can target

eIF5B would be of great importance. One such compound is LWW31, a small molecule ligand that has been suggested to interact with eIF5B and interfere with protein translation [148]. Treatment of hepatocellular carcinoma cells with LWW31 suggested that LWW31 is more cytotoxic to hepatocellular carcinoma cells than noncancerous cells [148], suggesting that eIF5B is a druggable target. Further efforts into the design of compounds that can interact with and interfere with the role of eIF5B in IRES-mediated translation would be of great value. In particular, targeting domain IV of eIF5B which is known to interact with $tRNA_i$ [75]would be of great importance.

In addition to OSCC, the impact of eIF5B in cancer formation and progression in other cancers has been identified. In GBM cells, eIF5B depletion was correlated with decreased levels of the antiapoptotic proteins cIAP1, XIAP, Bcl-xL, and cFLIPs [31]. GBM cells also exhibited increased sensitivity to TRAIL upon eIF5B depletion due to activation of apoptosis, as well as a decrease in p-65 levels [108], suggesting that eIF5B depletion is hindering NF-κB pathway activity as well. In lung cancer, the overexpression of eIF5B was found to upregulate levels of PD-L1, promoting immune evasion of lung cancer cells and thus promoting cancer survival and progression [88]. The expression of eIF5B and its effect on PD-L1 were also seen in prostate cancer cells as well [86], suggesting that eIF5B is aiding multiple cancer types in resisting immune responses. In addition to aiding in the evasion of immune responses, eIF5B expression has been correlated with aggressive phenotypes, shorter recurrence-free survival and increased proliferation and migration in hepatocellular carcinoma cells [89]. These reports suggest that eIF5B has the potential to be a valuable therapeutic target in multiple different cancer types.

eIF5B depletion has been shown to be beneficial in cancer cells, however, it is important to consider the potential limitations of eIF5B depletion and its off-target effects. During cap-

dependent transitions, eIF5B primarily mediates efficient interaction of the 40S and 60S subunits [73]. In addition to this, eIF5B has been reported to have other roles as well, including aiding in ribosome maturation, interacting with eIF5 to facilitate stable 48S pre-initiation complex formation, and interacting with eIF1A to stabilize $tRNA_i$ [75]. eIF5B has also been reported to aid in the regulation of cell cycle progression and thus depletion of eIF5B in eukaryotes has been shown to display a stunted growth phenotype [75].

In conclusion, our work suggests that eIF5B may be involved in OSCC cancer biology by playing a likely role in IRES-mediated translation. The reduction of anti-apoptotic proteins upon eIF5B depletion indicates that eIF5B depletion may hinder the evasion of apoptosis and promote cell death. The decreases in levels of VEGF, HIF-1α, and other markers of invasion, proliferation and migration suggest that eIF5B depletion may also slow proliferation, invasion, migration and invasion, as well as angiogenesis in OSCC cells. The presence of IRES elements in mRNAs of HIF-1α, VEGF and certain anti-apoptotic proteins may be how eIF5B is regulating their levels. Bioinformatic analyses have shown that eIF5B is a prognostic biomarker for OSCC and this work will aid in establishing eIF5B as a therapeutic target for OSCC treatment.

Future Directions

So far, the data generated has been from Cal33 cells, an OSCC cell line derived from differentiated squamous tongue carcinoma [149]. To gauge a better understanding of the effects of eIF5B depletion in OSCC, it may be beneficial to perform these experiments in OSCC cell lines derived from other anatomical locations. In our lab, we have access to UMSCC1 (floor of

mouth) and UMSCC29 (alveolar ridge) cell lines [150]. Performing experiments in these anatomically diverse cell lines may provide us with a clearer picture of how eIF5B depletion may affect OSCC cell survival, proliferation, invasion, and migration. In this body of work, I have shown a correlation between eIF5B depletion and decreases in antiapoptotic proteins and markers involved in proliferation, invasion, and migration. However, to show that these proteins are regulated by eIF5B at the translational level, polysome profiling experiments will have to be performed. At the translational level, mRNAs being translated more frequently will have more ribosomes bound to them. Using cycloheximide, ribosomes can be "frozen" onto the mRNAs in control or eIF5B depletion conditions. mRNAs with many ribosomes, referred to as polysomes, have high molecular weight and can be separated from mRNAs with few ribosomes or no ribosomes through centrifugation on a sucrose gradient [31,151]. Upon fraction collection and absorbance measurement, we can obtain a polysome profile revealing the presence of polysomes under control and eIF5B depletion conditions. The presence of less polysome under eIF5B depletion conditions suggests that the mRNA being analyzed is downregulated at the translational level. To confirm this is the case, reverse-transcriptase polymerase chain reaction (RT-PCR) can be performed to gauge steady-state levels of mRNAs under control and eIF5B depletion conditions. If the mRNA levels are similar between the two conditions, it can further suggest that any change we observe in protein expression is at the translational level. This study is restricted to looking into the role of eIF5B in regulating levels of anti-apoptotic proteins and markers of proliferation, invasion, migration, and angiogenesis as we cannot establish a direct link between eIF5B and IRES-mediated translation of these mRNAs. To better understand the role of eIF5B in OSCC pathophysiology, we will also need to perform ribosome profiling (RiboSeq) experiments.

Literatures Cited

1 Pekarek, L. *et al.* Emerging histological and serological biomarkers in oral squamous cell carcinoma: Applications in diagnosis, prognosis evaluation and personalized therapeutics (Review). *Oncol Rep* **50** (2023). https://doi.org:10.3892/or.2023.8650

2 Bose, P. *et al.* Tumor cell apoptosis mediated by cytoplasmic ING1 is associated with improved survival in oral squamous cell carcinoma patients. *Oncotarget* **5**, 3210-3219 (2014). https://doi.org:10.18632/oncotarget.1907

3 Tan, Y. *et al.* Oral squamous cell carcinomas: state of the field and emerging directions. *International Journal of Oral Science* **15**, 44 (2023). https://doi.org:10.1038/s41368-023-00249-w

4 Imbesi Bellantoni, M. *et al.* Oral Cavity Squamous Cell Carcinoma: An Update of the Pharmacological Treatment. *Biomedicines* **11** (2023). https://doi.org:10.3390/biomedicines11041112

5 Bugshan, A. & Farooq, I. Oral squamous cell carcinoma: metastasis, potentially associated malignant disorders, etiology and recent advancements in diagnosis. *F1000Res* **9**, 229 (2020). https://doi.org:10.12688/f1000research.22941.1

6 Yang, J. *et al.* Survival analysis of age-related oral squamous cell carcinoma: a population study based on SEER. *European Journal of Medical Research* **28**, 413 (2023). https://doi.org:10.1186/s40001-023-01345-7

7 Martínez-Barajas, M. G. *et al.* HPV-Negative and HPV-Positive Oral Cancer Cells Stimulate the Polarization of Neutrophils towards Different Functional Phenotypes In Vitro. *Cancers (Basel)* **15** (2023). https://doi.org:10.3390/cancers15245814

8 Shahar, N. & Larisch, S. Inhibiting the inhibitors: Targeting anti-apoptotic proteins in cancer and therapy resistance. *Drug Resist Updat* **52**, 100712 (2020). https://doi.org:10.1016/j.drup.2020.100712

9 Opferman, J. T. & Kothari, A. Anti-apoptotic BCL-2 family members in development. *Cell Death Differ* **25**, 37-45 (2018). https://doi.org:10.1038/cdd.2017.170

10 Krasovec, G., Horkan, H. R., Quéinnec, É. & Chambon, J.-P. The constructive function of apoptosis: More than a dead-end job. *Frontiers in Cell and Developmental Biology* **10** (2022). https://doi.org:10.3389/fcell.2022.1033645

11 Obeng, E. Apoptosis (programmed cell death) and its signals - A review. *Braz J Biol* **81**, 1133-1143 (2021). https://doi.org:10.1590/1519-6984.228437

12 Lossi, L. The concept of intrinsic versus extrinsic apoptosis. *Biochem J* **479**, 357-384 (2022). https://doi.org:10.1042/bcj20210854

13 Elmore, S. Apoptosis: a review of programmed cell death. *Toxicol Pathol* **35**, 495-516 (2007). https://doi.org:10.1080/01926230701320337

14 Ivanisenko, N. V. *et al.* Regulation of extrinsic apoptotic signaling by c-FLIP: towards targeting cancer networks. *Trends Cancer* **8**, 190-209 (2022). https://doi.org:10.1016/j.trecan.2021.12.002

15 Wallach, D. The Tumor Necrosis Factor Family: Family Conventions and Private Idiosyncrasies. *Cold Spring Harb Perspect Biol* **10** (2018). https://doi.org:10.1101/cshperspect.a028431

16 Wang, X. *et al.* Expression of cluster of differentiation-95 and relevant signaling molecules in liver cancer. *Mol Med Rep* **11**, 3375-3381 (2015). https://doi.org:10.3892/mmr.2014.3129

17 Safa, A. R. Roles of c-FLIP in Apoptosis, Necroptosis, and Autophagy. *J Carcinog Mutagen* **Suppl 6** (2013). https://doi.org:10.4172/2157-2518.S6-003

18 Mahdizadeh, S. J., Thomas, M. & Eriksson, L. A. Reconstruction of the Fas-Based Death-Inducing Signaling Complex (DISC) Using a Protein–Protein Docking Meta-Approach. *Journal of Chemical Information and Modeling* **61**, 3543-3558 (2021). https://doi.org:10.1021/acs.jcim.1c00301

19 Jan, R. & Chaudhry, G. E. Understanding Apoptosis and Apoptotic Pathways Targeted Cancer Therapeutics. *Adv Pharm Bull* **9**, 205-218 (2019). https://doi.org:10.15171/apb.2019.024

20 Beaudouin, J., Liesche, C., Aschenbrenner, S., Hörner, M. & Eils, R. Caspase-8 cleaves its substrates from the plasma membrane upon CD95-induced apoptosis. *Cell Death & Differentiation* **20**, 599-610 (2013). https://doi.org:10.1038/cdd.2012.156

21 Orning, P. & Lien, E. Multiple roles of caspase-8 in cell death, inflammation, and innate immunity. *J Leukoc Biol* **109**, 121-141 (2021). https://doi.org:10.1002/jlb.3mr0420-305r

22 Huang, K. *et al.* Cleavage by Caspase 8 and Mitochondrial Membrane Association Activate the BH3-only Protein Bid during TRAIL-induced Apoptosis. *J Biol Chem* **291**, 11843-11851 (2016). https://doi.org:10.1074/jbc.M115.711051

23 Moldoveanu, T. & Czabotar, P. E. BAX, BAK, and BOK: A Coming of Age for the BCL-2 Family Effector Proteins. *Cold Spring Harb Perspect Biol* **12** (2020). https://doi.org:10.1101/cshperspect.a036319

24 Peña-Blanco, A. & García-Sáez, A. J. Bax, Bak and beyond - mitochondrial performance in apoptosis. *Febs j* **285**, 416-431 (2018). https://doi.org:10.1111/febs.14186

25 Elena-Real, C. A. *et al.* Cytochrome c speeds up caspase cascade activation by blocking 14-3-3ε-dependent Apaf-1 inhibition. *Cell Death & Disease* **9**, 365 (2018). https://doi.org:10.1038/s41419-018-0408-1

26 Molyer, B., Kumar, A. & Angel, J. B. SMAC Mimetics as Therapeutic Agents in HIV Infection. *Front Immunol* **12**, 780400 (2021). https://doi.org:10.3389/fimmu.2021.780400

27 Dorstyn, L., Akey, C. W. & Kumar, S. New insights into apoptosome structure and function. *Cell Death Differ* **25**, 1194-1208 (2018). https://doi.org:10.1038/s41418-017-0025-z

28 Al-Aamri, H. M., Irving, H. R., Bradley, C. & Meehan-Andrews, T. Intrinsic and extrinsic apoptosis responses in leukaemia cells following daunorubicin treatment. *BMC Cancer* **21**, 438 (2021). https://doi.org:10.1186/s12885-021-08167-y

29 Mucci, S. *et al.* Acute severe hypoxia induces apoptosis of human pluripotent stem cells by a HIF-1α and P53 independent mechanism. *Scientific Reports* **12**, 18803 (2022). https://doi.org:10.1038/s41598-022-23650-7

30 Hussar, P. Apoptosis Regulators Bcl-2 and Caspase-3. *Encyclopedia* **2**, 1624-1636 (2022).

31 Ross, J. A. *et al.* Eukaryotic initiation factor 5B (eIF5B) provides a critical cell survival switch to glioblastoma cells via regulation of apoptosis. *Cell Death Dis* **10**, 57 (2019). https://doi.org:10.1038/s41419-018-1283-5

32 Safa, A. R., Kamocki, K., Saadatzadeh, M. R. & Bijangi-Vishehsaraei, K. c-FLIP, a Novel Biomarker for Cancer Prognosis, Immunosuppression, Alzheimer's Disease, Chronic Obstructive Pulmonary Disease (COPD), and a Rationale Therapeutic Target. *Biomark J* **5** (2019). https://doi.org:10.36648/2472-1646.5.1.59

33 Fox, J. L. *et al.* Cryo-EM structural analysis of FADD:Caspase-8 complexes defines the catalytic dimer architecture for co-ordinated control of cell fate. *Nature Communications* **12**, 819 (2021). https://doi.org:10.1038/s41467-020-20806-9

34 Graber, T. E. & Holcik, M. Distinct roles for the cellular inhibitors of apoptosis proteins 1 and 2. *Cell Death & Disease* **2**, e135-e135 (2011). https://doi.org:10.1038/cddis.2011.20

35 Lukacs, C. *et al.* The structure of XIAP BIR2: understanding the selectivity of the BIR domains. *Acta Crystallogr D Biol Crystallogr* **69**, 1717-1725 (2013). https://doi.org:10.1107/s0907444913016284

36 Obexer, P. & Ausserlechner, M. J. X-Linked Inhibitor of Apoptosis Protein – A Critical Death Resistance Regulator and Therapeutic Target for Personalized Cancer Therapy. *Frontiers in Oncology* **4** (2014). https://doi.org:10.3389/fonc.2014.00197

37 Li, M., Wang, D., He, J., Chen, L. & Li, H. Bcl-X(L): A multifunctional anti-apoptotic protein. *Pharmacol Res* **151**, 104547 (2020). https://doi.org:10.1016/j.phrs.2019.104547

38 Bai, L. *et al.* BM-1197: a novel and specific Bcl-2/Bcl-xL inhibitor inducing complete and long-lasting tumor regression in vivo. *PLoS One* **9**, e99404 (2014). https://doi.org:10.1371/journal.pone.0099404

39 Saha, T., Solomon, J., Samson, A. O. & Gil-Henn, H. Invasion and Metastasis as a Central Hallmark of Breast Cancer. *J Clin Med* **10** (2021). https://doi.org:10.3390/jcm10163498

40 Wu, J. S. *et al.* Plasticity of cancer cell invasion: Patterns and mechanisms. *Transl Oncol* **14**, 100899 (2021). https://doi.org:10.1016/j.tranon.2020.100899

41 Hanahan, D. & Weinberg, R. A. Hallmarks of cancer: the next generation. *Cell* **144**, 646-674 (2011). https://doi.org:10.1016/j.cell.2011.02.013

42 Matson, J. P. & Cook, J. G. Cell cycle proliferation decisions: the impact of single cell analyses. *Febs j* **284**, 362-375 (2017). https://doi.org:10.1111/febs.13898

43 Feitelson, M. A. *et al.* Sustained proliferation in cancer: Mechanisms and novel therapeutic targets. *Semin Cancer Biol* **35 Suppl**, S25-s54 (2015). https://doi.org:10.1016/j.semcancer.2015.02.006

44 Duronio, R. J. & Xiong, Y. Signaling pathways that control cell proliferation. *Cold Spring Harb Perspect Biol* **5**, a008904 (2013). https://doi.org:10.1101/cshperspect.a008904

45 Krakhmal, N. V., Zavyalova, M. V., Denisov, E. V., Vtorushin, S. V. & Perelmuter, V. M. Cancer Invasion: Patterns and Mechanisms. *Acta Naturae* **7**, 17-28 (2015).

46 Fares, J., Fares, M. Y., Khachfe, H. H., Salhab, H. A. & Fares, Y. Molecular principles of metastasis: a hallmark of cancer revisited. *Signal Transduction and Targeted Therapy* **5**, 28 (2020). https://doi.org:10.1038/s41392-020-0134-x

47 Sun, Y. *et al.* Signaling pathway of MAPK/ERK in cell proliferation, differentiation, migration, senescence and apoptosis. *J Recept Signal Transduct Res* **35**, 600-604 (2015). https://doi.org:10.3109/10799893.2015.1030412

48 Guo, Y. J. *et al.* ERK/MAPK signalling pathway and tumorigenesis. *Exp Ther Med* **19**, 1997-2007 (2020). https://doi.org:10.3892/etm.2020.8454

49 Wee, P. & Wang, Z. Epidermal Growth Factor Receptor Cell Proliferation Signaling Pathways. *Cancers (Basel)* **9** (2017). https://doi.org:10.3390/cancers9050052

50 Purba, E. R., Saita, E. I. & Maruyama, I. N. Activation of the EGF Receptor by Ligand Binding and Oncogenic Mutations: The "Rotation Model". *Cells* **6** (2017). https://doi.org:10.3390/cells6020013

51 Samson, S. C., Khan, A. M. & Mendoza, M. C. ERK signaling for cell migration and invasion. *Frontiers in Molecular Biosciences* **9** (2022). https://doi.org:10.3389/fmolb.2022.998475

52 Yang, W. S. *et al.* RSK1 and RSK2 serine/threonine kinases regulate different transcription programs in cancer. *Front Cell Dev Biol* **10**, 1015665 (2022). https://doi.org:10.3389/fcell.2022.1015665

53 Mebratu, Y. & Tesfaigzi, Y. How ERK1/2 activation controls cell proliferation and cell death: Is subcellular localization the answer? *Cell Cycle* **8**, 1168-1175 (2009). https://doi.org:10.4161/cc.8.8.8147

54 Jin, X., Dai, L., Ma, Y., Wang, J. & Liu, Z. Implications of HIF-1α in the tumorigenesis and progression of pancreatic cancer. *Cancer Cell International* **20**, 273 (2020). https://doi.org:10.1186/s12935-020-01370-0

55 Cimmino, F. *et al.* HIF-1 transcription activity: HIF1A driven response in normoxia and in hypoxia. *BMC Medical Genetics* **20**, 37 (2019). https://doi.org:10.1186/s12881-019-0767-1

56 Singh, S. & Singh, T. G. Role of Nuclear Factor Kappa B (NF-κB) Signalling in Neurodegenerative Diseases: An Mechanistic Approach. *Curr Neuropharmacol* **18**, 918-935 (2020). https://doi.org:10.2174/1570159x18666200207120949

57 Oeckinghaus, A. & Ghosh, S. The NF-kappaB family of transcription factors and its regulation. *Cold Spring Harb Perspect Biol* **1**, a000034 (2009). https://doi.org:10.1101/cshperspect.a000034

58 Yu, H., Lin, L., Zhang, Z., Zhang, H. & Hu, H. Targeting NF-κB pathway for the therapy of diseases: mechanism and clinical study. *Signal Transduction and Targeted Therapy* **5**, 209 (2020). https://doi.org:10.1038/s41392-020-00312-6

59 Liang, Y. *et al.* Effect of canonical NF-κB signaling pathway on the differentiation of rat dental epithelial stem cells. *Stem Cell Research & Therapy* **10**, 139 (2019). https://doi.org:10.1186/s13287-019-1252-7

60 Sun, S.-C. The non-canonical NF-κB pathway in immunity and inflammation. *Nature Reviews Immunology* **17**, 545-558 (2017). https://doi.org:10.1038/nri.2017.52

61 Trares, K., Ackermann, J. & Koch, I. The canonical and non-canonical NF-κB pathways and their crosstalk: A comparative study based on Petri nets. *Biosystems* **211**, 104564 (2022). https://doi.org:https://doi.org/10.1016/j.biosystems.2021.104564

62 Xia, Y., Shen, S. & Verma, I. M. NF-κB, an active player in human cancers. *Cancer Immunol Res* **2**, 823-830 (2014). https://doi.org:10.1158/2326-6066.Cir-14-0112

63 Liu, Z.-L., Chen, H.-H., Zheng, L.-L., Sun, L.-P. & Shi, L. Angiogenic signaling pathways and anti-angiogenic therapy for cancer. *Signal Transduction and Targeted Therapy* **8**, 198 (2023). https://doi.org:10.1038/s41392-023-01460-1

64 Kwon, H.-J. *et al.* Stepwise phosphorylation of p65 promotes NF-κB activation and NK cell responses during target cell recognition. *Nature Communications* **7**, 11686 (2016). https://doi.org:10.1038/ncomms11686

65 Wang, R. *et al.* MCPIP1 promotes cell proliferation, migration and angiogenesis of glioma via VEGFA-mediated ERK pathway. *Experimental Cell Research* **418**, 113267 (2022). https://doi.org:https://doi.org/10.1016/j.yexcr.2022.113267

66 Leibovitch, M. & Topisirovic, I. Dysregulation of mRNA translation and energy metabolism in cancer. *Adv Biol Regul* **67**, 30-39 (2018). https://doi.org:10.1016/j.jbior.2017.11.001

67 Pandolfi, P. P. Aberrant mRNA translation in cancer pathogenesis: an old concept revisited comes finally of age. *Oncogene* **23**, 3134-3137 (2004). https://doi.org:10.1038/sj.onc.1207618

68 Robichaud, N., Sonenberg, N., Ruggero, D. & Schneider, R. J. Translational Control in Cancer. *Cold Spring Harb Perspect Biol* **11** (2019). https://doi.org:10.1101/cshperspect.a032896

69 Martínez-Salas, E. *et al.* RNA-binding proteins impacting on internal initiation of translation. *Int J Mol Sci* **14**, 21705-21726 (2013). https://doi.org:10.3390/ijms141121705

70 Durie, D., Hatzoglou, M., Chakraborty, P. & Holcik, M. HuR controls mitochondrial morphology through the regulation of Bcl(xL) translation. *Translation (Austin)* **1** (2013). https://doi.org:10.4161/trla.23980

71 Mohamad, I. *et al.* Current Treatment Strategies and Risk Stratification for Oral Carcinoma. *American Society of Clinical Oncology Educational Book*, e389810 (2023). https://doi.org:10.1200/edbk_389810

72 Kim, H. J. Cell Fate Control by Translation: mRNA Translation Initiation as a Therapeutic Target for Cancer Development and Stem Cell Fate Control. *Biomolecules* **9** (2019). https://doi.org:10.3390/biom9110665

73 Sharma, D. K., Bressler, K., Patel, H., Balasingam, N. & Thakor, N. Role of Eukaryotic Initiation Factors during Cellular Stress and Cancer Progression. *J Nucleic Acids* **2016**, 8235121 (2016). https://doi.org:10.1155/2016/8235121

74 Baird, T. D. & Wek, R. C. Eukaryotic Initiation Factor 2 Phosphorylation and Translational Control in Metabolism. *Advances in Nutrition* **3**, 307-321 (2012). https://doi.org:https://doi.org/10.3945/an.112.002113

75 Chukka, P. A. R., Wetmore, S. D. & Thakor, N. Established and Emerging Regulatory Roles of Eukaryotic Translation Initiation Factor 5B (eIF5B). *Front Genet* **12**, 737433 (2021). https://doi.org:10.3389/fgene.2021.737433

76 Thakor, N. & Holcik, M. IRES-mediated translation of cellular messenger RNA operates in eIF2α- independent manner during stress. *Nucleic Acids Research* **40**, 541-552 (2011). https://doi.org:10.1093/nar/gkr701

77 Sharma, D. K., Bressler, K., Patel, H., Balasingam, N. & Thakor, N. Role of Eukaryotic Initiation Factors during Cellular Stress and Cancer Progression. *Journal of Nucleic Acids* **2016**, 8235121 (2016). https://doi.org:10.1155/2016/8235121

78 Zhao, E. M. *et al.* RNA-responsive elements for eukaryotic translational control. *Nature Biotechnology* **40**, 539-545 (2022). https://doi.org:10.1038/s41587-021-01068-2

79 Kwan, T. & Thompson, S. R. Noncanonical Translation Initiation in Eukaryotes. *Cold Spring Harb Perspect Biol* **11** (2019). https://doi.org:10.1101/cshperspect.a032672

80 Yang, Y. & Wang, Z. IRES-mediated cap-independent translation, a path leading to hidden proteome. *J Mol Cell Biol* **11**, 911-919 (2019). https://doi.org:10.1093/jmcb/mjz091

81 Xue, S. & Barna, M. Cis-regulatory RNA elements that regulate specialized ribosome activity. *RNA Biology* **12**, 1083-1087 (2015). https://doi.org:10.1080/15476286.2015.1085149

82 Lozano, G., Francisco-Velilla, R. & Martinez-Salas, E. Ribosome-dependent conformational flexibility changes and RNA dynamics of IRES domains revealed by differential SHAPE. *Scientific Reports* **8**, 5545 (2018). https://doi.org:10.1038/s41598-018-23845-x

83 Komar, A. A. & Hatzoglou, M. Cellular IRES-mediated translation: the war of ITAFs in pathophysiological states. *Cell Cycle* **10**, 229-240 (2011). https://doi.org:10.4161/cc.10.2.14472

84 Chee, N. T., Lohse, I. & Brothers, S. P. mRNA-to-protein translation in hypoxia. *Molecular Cancer* **18**, 49 (2019). https://doi.org:10.1186/s12943-019-0968-4

85 Ho, J. J. D. *et al.* Oxygen-Sensitive Remodeling of Central Carbon Metabolism by Archaic eIF5B. *Cell Rep* **22**, 17-26 (2018). https://doi.org:10.1016/j.celrep.2017.12.031

86 Li, Q. *et al.* eIF5B regulates the expression of PD-L1 in prostate cancer cells by interacting with Wig1. *BMC Cancer* **21**, 1022 (2021). https://doi.org:10.1186/s12885-021-08749-w

87 Han, Y., Liu, D. & Li, L. PD-1/PD-L1 pathway: current researches in cancer. *Am J Cancer Res* **10**, 727-742 (2020).

88 Suresh, S. *et al.* eIF5B drives integrated stress response-dependent translation of PD-L1 in lung cancer. *Nat Cancer* **1**, 533-545 (2020). https://doi.org:10.1038/s43018-020-0056-0

89 Wang, Z. G. *et al.* eIF5B increases ASAP1 expression to promote HCC proliferation and invasion. *Oncotarget* **7**, 62327-62339 (2016). https://doi.org:10.18632/oncotarget.11469

90 De la Cruz-Morcillo, M. A. *et al.* p75 neurotrophin receptor and pro-BDNF promote cell survival and migration in clear cell renal cell carcinoma. *Oncotarget* **7**, 34480-34497 (2016). https://doi.org:10.18632/oncotarget.8911

91 Kröplin, J. & Reppenhagen, J. C. Best practices and future challenges in the treatment of oral cancer. *Innov Surg Sci* **8**, 215-220 (2023). https://doi.org:10.1515/iss-2023-0031

92 Law, Z.-J. *et al.* Extracellular Vesicle-Mediated Chemoresistance in Oral Squamous Cell Carcinoma. *Frontiers in Molecular Biosciences* **8** (2021). https://doi.org:10.3389/fmolb.2021.629888

93 He, S., Chakraborty, R. & Ranganathan, S. Proliferation and Apoptosis Pathways and Factors in Oral Squamous Cell Carcinoma. *Int J Mol Sci* **23** (2022). https://doi.org:10.3390/ijms23031562

94 Fan, T. *et al.* NUPR1 promotes the proliferation and metastasis of oral squamous cell carcinoma cells by activating TFE3-dependent autophagy. *Signal Transduction and Targeted Therapy* **7**, 130 (2022). https://doi.org:10.1038/s41392-022-00939-7

95 Lin, Y. *et al.* ENO1 Promotes OSCC Migration and Invasion by Orchestrating IL-6 Secretion from Macrophages via a Positive Feedback Loop. *Int J Mol Sci* **24** (2023). https://doi.org:10.3390/ijms24010737

96 Cheng, Y., Li, S., Gao, L., Zhi, K. & Ren, W. The Molecular Basis and Therapeutic Aspects of Cisplatin Resistance in Oral Squamous Cell Carcinoma. *Front Oncol* **11**, 761379 (2021). https://doi.org:10.3389/fonc.2021.761379

97 Shriwas, O. *et al.* RRBP1 rewires cisplatin resistance in oral squamous cell carcinoma by regulating Hippo pathway. *British Journal of Cancer* **124**, 2004-2016 (2021). https://doi.org:10.1038/s41416-021-01336-7

98 Khoo, X. H., Paterson, I. C., Goh, B. H. & Lee, W. L. Cisplatin-Resistance in Oral Squamous Cell Carcinoma: Regulation by Tumor Cell-Derived Extracellular Vesicles. *Cancers (Basel)* **11** (2019). https://doi.org:10.3390/cancers11081166

99 Montiel-Dávalos, A., Ayala, Y. & Hernández, G. The dark side of mRNA translation and the translation machinery in glioblastoma. *Frontiers in Cell and Developmental Biology* **11** (2023). https://doi.org:10.3389/fcell.2023.1086964

100 Wang, Y. *et al.* Expanding uncapped translation and emerging function of circular RNA in carcinomas and noncarcinomas. *Molecular Cancer* **21**, 13 (2022). https://doi.org:10.1186/s12943-021-01484-7

101 Sriram, A., Bohlen, J. & Teleman, A. A. Translation acrobatics: how cancer cells exploit alternate modes of translational initiation. *EMBO Rep* **19** (2018). https://doi.org:10.15252/embr.201845947

102 Rubio, A., Garland, G. D., Sfakianos, A., Harvey, R. F. & Willis, A. E. Aberrant protein synthesis and cancer development: The role of canonical eukaryotic initiation, elongation and termination factors in tumorigenesis. *Seminars in Cancer Biology* **86**, 151-165 (2022). https://doi.org:https://doi.org/10.1016/j.semcancer.2022.04.006

103 Xue, S. & Barna, M. Cis-regulatory RNA elements that regulate specialized ribosome activity. *RNA Biol* **12**, 1083-1087 (2015). https://doi.org:10.1080/15476286.2015.1085149

104 Gu, L. *et al.* Regulation of XIAP translation and induction by MDM2 following irradiation. *Cancer Cell* **15**, 363-375 (2009). https://doi.org:10.1016/j.ccr.2009.03.002

105 Gu, L. *et al.* Discovery of Dual Inhibitors of MDM2 and XIAP for Cancer Treatment. *Cancer Cell* **30**, 623-636 (2016). https://doi.org:https://doi.org/10.1016/j.ccell.2016.08.015

106 Graber, T. E., Baird, S. D., Kao, P. N., Mathews, M. B. & Holcik, M. NF45 functions as an IRES trans-acting factor that is required for translation of cIAP1 during the unfolded protein response. *Cell Death Differ* **17**, 719-729 (2010). https://doi.org:10.1038/cdd.2009.164

107 Yosef, R. *et al.* Directed elimination of senescent cells by inhibition of BCL-W and BCL-XL. *Nature Communications* **7**, 11190 (2016). https://doi.org:10.1038/ncomms11190

108 van Zijl, F., Krupitza, G. & Mikulits, W. Initial steps of metastasis: cell invasion and endothelial transmigration. *Mutat Res* **728**, 23-34 (2011). https://doi.org:10.1016/j.mrrev.2011.05.002

109 Deka, K. & Li, Y. Transcriptional Regulation during Aberrant Activation of NF-κB Signalling in Cancer. *Cells* **12** (2023). https://doi.org:10.3390/cells12050788

110 Shibuya, M. Vascular Endothelial Growth Factor (VEGF) and Its Receptor (VEGFR) Signaling in Angiogenesis: A Crucial Target for Anti- and Pro-Angiogenic Therapies. *Genes Cancer* **2**, 1097-1105 (2011). https://doi.org:10.1177/1947601911423031

111 Lang, K. *et al.* Definitive radiotherapy for squamous cell carcinoma of the oral cavity: a single-institution experience. *Radiology and Oncology* **55**, 467-473 (2021). https://doi.org:doi:10.2478/raon-2021-0041

112 Ferreira, A. K. *et al.* Survival and prognostic factors in patients with oral squamous cell carcinoma. *Med Oral Patol Oral Cir Bucal* **26**, e387-e392 (2021). https://doi.org:10.4317/medoral.24242

113 Meril, S. *et al.* Loss-of-function cancer-linked mutations in the EIF4G2 non-canonical translation initiation factor. *Life Science Alliance* **7**, e202302338 (2024). https://doi.org:10.26508/lsa.202302338

114 Grove, D. J., Russell, P. J. & Kearse, M. G. To initiate or not to initiate: A critical assessment of eIF2A, eIF2D, and MCT-1·DENR to deliver initiator tRNA to ribosomes. *WIREs RNA* **15**, e1833 (2024). https://doi.org:https://doi.org/10.1002/wrna.1833

115 Crowley, L. C., Marfell, B. J., Scott, A. P. & Waterhouse, N. J. Quantitation of Apoptosis and Necrosis by Annexin V Binding, Propidium Iodide Uptake, and Flow Cytometry. *Cold Spring Harb Protoc* **2016** (2016). https://doi.org:10.1101/pdb.prot087288

116 Nagata, S., Suzuki, J., Segawa, K. & Fujii, T. Exposure of phosphatidylserine on the cell surface. *Cell Death & Differentiation* **23**, 952-961 (2016). https://doi.org:10.1038/cdd.2016.7

117 Chazotte, B. Labeling nuclear DNA with hoechst 33342. *Cold Spring Harb Protoc* **2011**, pdb.prot5557 (2011). https://doi.org:10.1101/pdb.prot5557

118 Majtnerová, P. & Roušar, T. An overview of apoptosis assays detecting DNA fragmentation. *Mol Biol Rep* **45**, 1469-1478 (2018). https://doi.org:10.1007/s11033-018-4258-9

119 Caruso, S. *et al.* Defining the role of cytoskeletal components in the formation of apoptopodia and apoptotic bodies during apoptosis. *Apoptosis* **24**, 862-877 (2019). https://doi.org:10.1007/s10495-019-01565-5

120 Mead, T. J. & Lefebvre, V. Proliferation assays (BrdU and EdU) on skeletal tissue sections. *Methods Mol Biol* **1130**, 233-243 (2014). https://doi.org:10.1007/978-1-62703-989-5_17

121 Qian, C. N., Mei, Y. & Zhang, J. Cancer metastasis: issues and challenges. *Chin J Cancer* **36**, 38 (2017). https://doi.org:10.1186/s40880-017-0206-7

122 Gerstberger, S., Jiang, Q. & Ganesh, K. Metastasis. *Cell* **186**, 1564-1579 (2023). https://doi.org:10.1016/j.cell.2023.03.003

123 Devanaboyina, M. *et al.* NF-κB Signaling in Tumor Pathways Focusing on Breast and Ovarian Cancer. *Oncology Reviews* **16** (2022). https://doi.org:10.3389/or.2022.10568

124 Zhi, Y. *et al.* NF-κB signaling pathway confers neuroblastoma cells migration and invasion ability via the regulation of CXCR4. *Med Sci Monit* **20**, 2746-2752 (2014). https://doi.org:10.12659/msm.892597

125 McCain, J. The MAPK (ERK) Pathway: Investigational Combinations for the Treatment Of BRAF-Mutated Metastatic Melanoma. *P t* **38**, 96-108 (2013).

126 Orton, R. J. *et al.* Computational modelling of cancerous mutations in the EGFR/ERK signalling pathway. *BMC Systems Biology* **3**, 100 (2009). https://doi.org:10.1186/1752-0509-3-100

127 Lin, S. *et al.* Redundant roles of EGFR ligands in the ERK activation waves during collective cell migration. *Life Sci Alliance* **5** (2022). https://doi.org:10.26508/lsa.202101206

128 Wortzel, I. & Seger, R. The ERK Cascade: Distinct Functions within Various Subcellular Organelles. *Genes Cancer* **2**, 195-209 (2011). https://doi.org:10.1177/1947601911407328

129 Jiang, W., Wang, X., Zhang, C., Xue, L. & Yang, L. Expression and clinical significance of MAPK and EGFR in triple-negative breast cancer. *Oncol Lett* **19**, 1842-1848 (2020). https://doi.org:10.3892/ol.2020.11274

130 Webb, T. E., Hughes, A., Smalley, D. S. & Spriggs, K. A. An internal ribosome entry site in the 5′ untranslated region of epidermal growth factor receptor allows hypoxic expression. *Oncogenesis* **4**, e134-e134 (2015). https://doi.org:10.1038/oncsis.2014.43

131 Badawi, Y. & Shi, H. Relative Contribution of Prolyl Hydroxylase-Dependent and -Independent Degradation of HIF-1alpha by Proteasomal Pathways in Cerebral Ischemia. *Frontiers in Neuroscience* **11** (2017). https://doi.org:10.3389/fnins.2017.00239

132 Abdi Sarabi, M. *et al.* Normoxic HIF-1α Stabilization Caused by Local Inflammatory Factors and Its Consequences in Human Coronary Artery Endothelial Cells. *Cells* **11** (2022). https://doi.org:10.3390/cells11233878

133 Park, M. H. & Hong, J. T. Roles of NF-κB in Cancer and Inflammatory Diseases and Their Therapeutic Approaches. *Cells* **5** (2016). https://doi.org:10.3390/cells5020015

134 Liu, T., Zhang, L., Joo, D. & Sun, S.-C. NF-κB signaling in inflammation. *Signal Transduction and Targeted Therapy* **2**, 17023 (2017). https://doi.org:10.1038/sigtrans.2017.23

135 Chen, S. *et al.* RelA/p65 inhibition prevents tendon adhesion by modulating inflammation, cell proliferation, and apoptosis. *Cell Death & Disease* **8**, e2710-e2710 (2017). https://doi.org:10.1038/cddis.2017.135

136 Zinatizadeh, M. R. *et al.* The Nuclear Factor Kappa B (NF-kB) signaling in cancer development and immune diseases. *Genes & Diseases* **8**, 287-297 (2021). https://doi.org:https://doi.org/10.1016/j.gendis.2020.06.005

137 Shostak, K. & Chariot, A. EGFR and NF-κB: partners in cancer. *Trends Mol Med* **21**, 385-393 (2015). https://doi.org:10.1016/j.molmed.2015.04.001

138 Wang, G. *et al.* ROS mediated EGFR/MEK/ERK/HIF-1α Loop Regulates Glucose metabolism in pancreatic cancer. *Biochem Biophys Res Commun* **500**, 873-878 (2018). https://doi.org:10.1016/j.bbrc.2018.04.177

139 Shi, J. & Wei, P. K. Interleukin-8: A potent promoter of angiogenesis in gastric cancer. *Oncol Lett* **11**, 1043-1050 (2016). https://doi.org:10.3892/ol.2015.4035

140 Li, A., Dubey, S., Varney, M. L., Dave, B. J. & Singh, R. K. IL-8 Directly Enhanced Endothelial Cell Survival, Proliferation, and Matrix Metalloproteinases Production and Regulated Angiogenesis1. *The Journal of Immunology* **170**, 3369-3376 (2003). https://doi.org:10.4049/jimmunol.170.6.3369

141 Wu, M. H. *et al.* Endothelin-1 promotes vascular endothelial growth factor-dependent angiogenesis in human chondrosarcoma cells. *Oncogene* **33**, 1725-1735 (2014). https://doi.org:10.1038/onc.2013.109

142 Nejabati, H. R., Latifi, Z., Ghasemnejad, T., Fattahi, A. & Nouri, M. Placental growth factor (PlGF) as an angiogenic/inflammatory switcher: lesson from early pregnancy losses. *Gynecol Endocrinol* **33**, 668-674 (2017). https://doi.org:10.1080/09513590.2017.1318375

143 Niu, G. & Chen, X. Vascular endothelial growth factor as an anti-angiogenic target for cancer therapy. *Curr Drug Targets* **11**, 1000-1017 (2010). https://doi.org:10.2174/138945010791591395

144 Li, Z. *et al.* Live-cell imaging-based dynamic vascular formation assay for antivascular drug evaluation and screening. *iScience* **26**, 106721 (2023). https://doi.org:https://doi.org/10.1016/j.isci.2023.106721

145 Zimna, A. & Kurpisz, M. Hypoxia-Inducible Factor-1 in Physiological and Pathophysiological Angiogenesis: Applications and Therapies. *Biomed Res Int* **2015**, 549412 (2015). https://doi.org:10.1155/2015/549412

146 Rao, D. D., Vorhies, J. S., Senzer, N. & Nemunaitis, J. siRNA vs. shRNA: Similarities and differences. *Advanced Drug Delivery Reviews* **61**, 746-759 (2009). https://doi.org:https://doi.org/10.1016/j.addr.2009.04.004

147 Deng, J., Bai, X., Tang, H. & Pang, S. DNA damage promotes ER stress resistance through elevation of unsaturated phosphatidylcholine in Caenorhabditis elegans. *J Biol Chem* **296**, 100095 (2021). https://doi.org:10.1074/jbc.RA120.016083

148 Wu, C. Y. *et al.* Rapid Discovery of Functional Small Molecule Ligands against Proteomic Targets through Library-Against-Library Screening. *ACS Comb Sci* **18**, 320-329 (2016). https://doi.org:10.1021/acscombsci.5b00194

149 Bauer, V. L. *et al.* Establishment and Molecular Cytogenetic Characterization of a Cell Culture Model of Head and Neck Squamous Cell Carcinoma (HNSCC). *Genes (Basel)* **1**, 388-412 (2010). https://doi.org:10.3390/genes1030388

150 Ludwig, M. L. *et al.* The genomic landscape of UM-SCC oral cavity squamous cell carcinoma cell lines. *Oral Oncol* **87**, 144-151 (2018). https://doi.org:10.1016/j.oraloncology.2018.10.031

151 Pereira, I. T. *et al.* Polysome profiling followed by RNA-seq of cardiac differentiation stages in hESCs. *Scientific Data* **5**, 180287 (2018). https://doi.org:10.1038/sdata.2018.287